Spring 4-25-2016

Binding of Oxygen to Human Hemoglobin Within the Erythrocyte Using ICAM Spectrophotometry

Kyle K. Hill
University of Nebraska-Lincoln, kyhill3@gmail.com

BINDING OF OXYGEN TO HUMAN HEMOGLOBIN WITHIN THE ERYTHROCYTE USING ICAM SPECTROPHOTOMETRY

by

Kyle Kelly Hill

A THESIS

Presented to the Faculty of

The Graduate College at the University of Nebraska

In Partial Fulfillment of Requirements

For the Degree of Master of Science

Major: Chemistry

Under the Supervision of Professor Lawrence J. Parkhurst

Lincoln, Nebraska

April, 2016

BINDING OF OXYGEN TO HUMAN HEMOGLOBIN WITHIN THE ERYTHROCYTE USING ICAM SPECTROPHOTOMETRY

Kyle Kelly Hill, M.S.

University of Nebraska, 2016

Advisor: Lawrence J. Parkhurst

Many of the spectrophotometric techniques used to determine the properties of intracellular human hemoglobin cannot be utilized due to the turbidity of erythrocyte suspensions. An Integrating Cavity Absorption Meter, or ICAM, allows for absorption measurements of strongly scattering samples in the visible-light region of the spectrum. The spectrum of oxygenated hemoglobin within erythrocytes is significantly different from the absorption spectrum of oxygenated hemoglobin in solution. Studies of the oxygen binding to hemoglobin in erythrocytes allowed the four sequential binding constants (Adair constants) to be determined and compared with those of hemoglobin in solution. The Adair constants for hemoglobin in solution were found to be markedly different from those of hemoglobin in the erythrocyte.

Acknowledgements

I would like to thank my advisor, Dr. Lawrence Parkhurst, for his support and encouragement. I would like to thank my family, for their support. I owe a debt to Tia Harris, without her support and love this would not be possible.

Table of Contents

Table of Figures

Table of Tables

Chapter 1 Introduction to Hemoglobin

1.1 The Structure of Hemoglobin

In 1959, Perutz elucidated the structure of horse hemoglobin using x-ray crystallography techniques, and in 1963 revealed the structure of human hemoglobin.[1,2] Adult hemoglobin consists of two α-globins and two β-globins which each contain a heme group. The heme is a porphyrin ring with an iron atom at its center. The tertiary structure refers to a polypeptide backboard with multiple structural components, while the quaternary structure refers to the interaction of multiple polypeptides within the same structure. There are two conformations of the heme globins; the *T*-state and the *R*-state. In the *R*-state, its oxygenated form, the heme lies in an isolated packet where it is tightly wedged between the 16 side chains of the globin. This allows no movement of the iron from the plane of the porphyrin ring. The iron forms 6-coordinates: four bonds to the porphyrin ring, one bond to histidine, and the sixth to the oxygen. In the deoxygenated *T*-state, the iron is in its 5 coordinated form, and the iron becomes displaced from the porphyrin plane by 0.4 Å.[3] The *T*-state is obstructed by the distal valine on the ligation side, and this obstruction cannot be cleared without a change in the polypeptide structure. Within these two different conformations, the globins determine the relationship of the iron within the porphyrin ring. As pointed out by Perutz and others, the dominant structural change between all four globins can be described as the $\alpha_1\beta_1$ and $\alpha_2\beta_2$ dimers remaining rigid while the contacts between $\alpha_1\beta_2$, $\alpha_2\beta_1$, $\alpha_1\alpha_2$, and $\beta_1\beta_2$ move relative to each other.[2,4] During deoxygenation, the $\alpha_1\alpha_2$, $\alpha_1\beta_1$, and $\alpha_2\beta_2$ heme distances remain stationary while the $\alpha_1\beta_1$ and $\alpha_2\beta_2$ act as hinges for the $\beta_1\beta_2$ heme distance increases 5Å (*fig. 1.1 and*

1.2).[5] The increase of the hemoglobin during the oxy-to-deoxy transition has been termed a "molecular lung in reverse."[3]

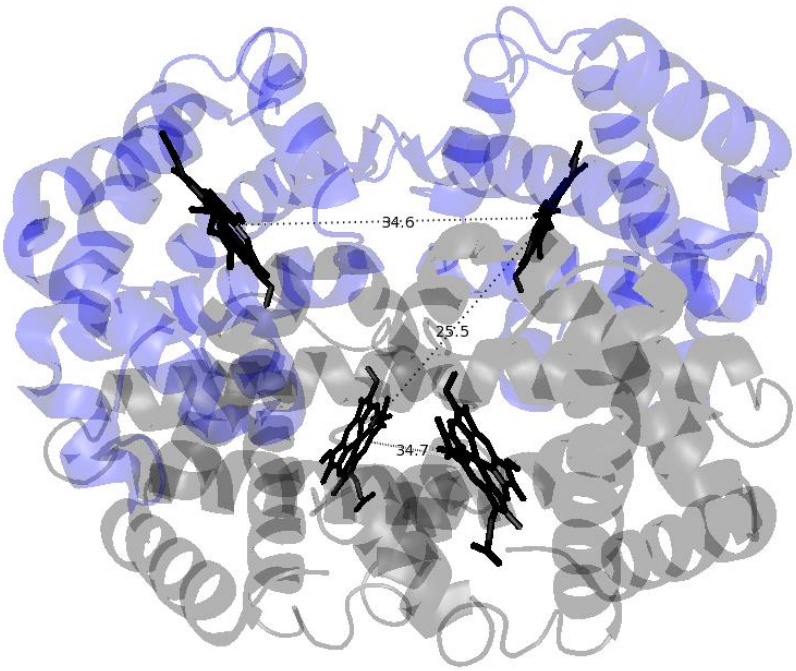

Figure 1.1: Molecular Lung in Reverse: Oxyhemoglobin

The α-globins are shown in transparent black, and the β-globins are shown in transparent blue. The heme groups are represented in solid black.

Structure	Distance
$Fe\beta_1$ - $Fe\beta_2$	34.6 Å
$Fe\alpha_1$ - $Fe\beta_2$	25.5 Å
$Fe\alpha_1$ - $Fe\alpha_2$	34.7 Å

Table 1.1: Heme Iron Distances in Oxyhemoglobin

The heme iron distances remain consistent during the oxy-deoxy transition of hemoglobin, except for the $Fe\beta_1$ - $Fe\beta_2$ heme distances, which increase 5 Å.

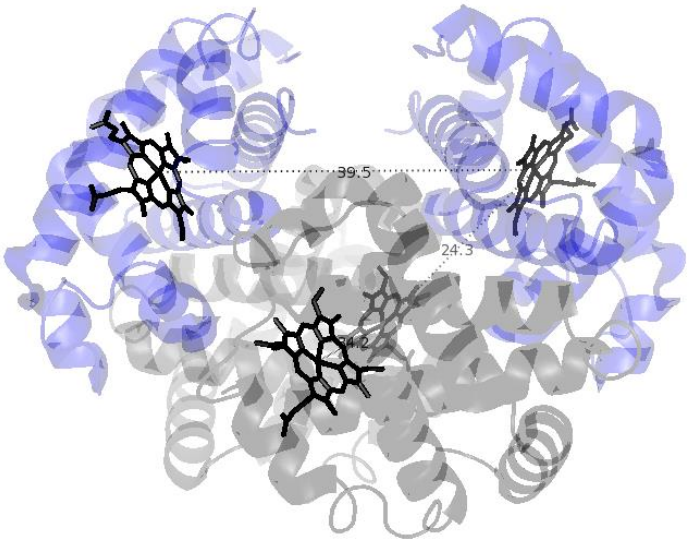

Figure 1.2: Molecular Lung in Reverse: Deoxyhemoglobin

The α-globins are shown in transparent black, and the β-globins are shown in transparent blue. The heme groups are represented in solid black.

Structure	Distance
$Fe\beta_1$ - $Fe\beta_2$	39.5 Å
$Fe\alpha_1$ - $Fe\beta_2$	24.3 Å
$Fe\alpha_1$ - $Fe\alpha_2$	34.2 Å

Table 1.2: Heme Iron Distances in Deoxyhemoglobin

The heme iron distances remain consistent during the oxy-deoxy transition of hemoglobin, except for the $Fe\beta_1$ - $Fe\beta_2$ heme distances, which increase 5 Å**.**

1.2 The History of Hemoglobin Research

Hemoglobin has been of great interest to the scientific community for the past two hundred years. In 1825, Engelhart showed that the iron-to-protein ratio in hemoglobin was similar across multiple species.[6] In 1878, Bert gave the first crude measurements of oxygen binding affinity.[7] In 1890, Hüfner crystallized both oxyhemoglobin and deoxyhemoglobin. When the deoxyhemoglobin crystal was exposed to oxygen, the crystals shattered, indicating a change in the size and conformation of the hemoglobin. Gasometric measurements in 1909 and 1922 were used by Barcroft, Haldane, and coworkers to study the thermodynamics of hemoglobin.[8,9] In 1924, Adair's dialysis experiments determined the molecular weight of hemoglobin.[10] At the time, the molecular weight of each globin was known to be 16,000, but the multiple of the globins was unknown. Adair determined the four globins of hemoglobin by comparing the molecular weight of each globin to the molecular weight of hemoglobin and the percent iron in the protein. In 1924, the refined gasometric measurements by Adair and others were the first attempts to determine sequential binding constants, the Adair constants, to be determined for mammalian hemoglobins.[11,12] With Adair's work, the tetrameric nature of hemoglobin was discovered, the molecular mass of the tetramer protein found, and the initial groundwork for the binding constants laid.

(1)
$$\bar{Y} = \frac{1}{4} * \frac{K_I[x]+2K_1K_2[x]^2+3K_1K_2K_3[x]^3+4K_1K_2K_3K_4[x]^4}{1+K_1[x]+K_1K_2[x]^2+K_1K_2K_3[x]^3+K_1K_2K_3K_4[x]^4}$$

Where $\bar{Y}$ represents the oxygen saturation of the hemoglobin and *x* represents the oxygen concentration.

Gasometric techniques can be described using a Van Slyke apparatus.[13] The Van Slyke apparatus uses a roundbottom flask filled with a solution of deoxygenated hemoglobin. A measured amount of air with oxygen is introduced to the flask, and given time to equilibrate. A small drop in the pressure indicated the binding of oxygen to hemoglobin. The gasometric measurements take considerable amounts of time, and are prone to high percent errors for the Adair constants.

Following the development of spectrophotometers, the ground work for tonometric methods, thin-layers and automated methods were developed in which the oxygen concentration was determined by dilution factors, calibrated flow methods, or by oxygen electrodes.[14-16] These techniques provided more precise data points, allowed multiple measurements per sample, and required much less protein, resulting in the replacement of the gasometric methods. Two of the methods related to our work are included below.

1.3 Imai's Hemoglobin Research

Imai, often considered Adair's protégé, worked extensively on the ligand-binding properties of hemoglobin. In the 1970s and 1980s, Imai *et. al.* developed a method to study the functional properties of abnormal hemoglobin, and later improved this method to determine the oxygen-hemoglobin equilibrium curves.[17] The Imai method uses the absorbance changes of hemoglobin at a single wavelength to determine the oxygen saturation, and using an oxygen electrode to determine the oxygen concentration. A solution of oxyhemoglobin is placed into a cell with magnetic stirring. The cell is placed in the path of a double-beam spectrophotometer with the path length ranging from 5 to 25

mm. The temperature is controlled by water circulating around the cell. A small thermistor is placed within the cell to measure the temperature of the sample. The gas phase above the liquid is filled and continuously replaced with argon or nitrogen, and the dissolved oxygen is removed from the solution. The fractional saturation of the hemoglobin is calculated via:

(2) $$\bar{Y} = [Abs(x) - Abs(0)]/[Abs(\infty) - Abs(0)]$$

Where $\bar{Y}$ represents the fractional saturation of hemoglobin by oxygen, $Abs_{(x)}$ represents the absorbance at a particular wavelength at a given oxygen concentration, $Abs_{(0)}$ represents the absorbance at a particular wavelength where the hemoglobin is fully deoxygenated, and $Abs_{(\infty)}$ represents the absorbance at a particular wavelength where the hemoglobin is fully oxygenated. Imai's body of work resulted in a number of studies reporting free energy changes for the successive steps of oxygenation for hemoglobin underneath a variety of conditions.[18]

1.4 Parkhurst's, Larsen's, and Meuser's Hemoglobin Research

Parkhurst *et. al.* worked to refine Imai's method by including an enzymatic system as well as a new method for oxygen concentration detection. This would ensure homogenous deoxygenation throughout the sample, eliminating the lag time from the gas-liquid equilibration from previous techniques. Parkhurst's initial aim was to develop an instrument that would allow rapid and continuous determinations of both fractional saturation and oxygen depletion by spectrophotometry.[19] Two enzyme systems were used: 1) glucose oxidase with beta-D-glucose in the presence of catalase, or 2) protocatechuate-3,4-dioxygenase in the presence of protocatechuic acid.[20,21] The

hemoglobin sample was loaded into a stopped-flow cuvette with two syringes, which were both filled with oxymyoglobin, bovine serum alblumin and dithiothreitol. When glucose oxidase was used to deoxygenate the sample, the first syringe also contained catalase and glucose, while second syringe contained glucose oxidase. When protocatechuate-3,4-dioxygenase was used to deoxygenate the sample, the first syringe contained protocatechuic acid and the second syringe contained protocatechuqte-3,4-dioxygenase. In their initial set-up, the oxygen activity was detected using myoglobin, and the spectrophotometer oscillated between reading the absorbance at 585.9 nm, the isosbestic point for oxyhemoglobin and deoxyhemoglobin, and the absorbance at 590.6 nm, the isosbestic point for oxymyoglobin and deoxymyoglobin. 375 data pairs were collected over the 25-minute duration of the hemoglobin deoxygenation, then continued for an additional 40 minutes until the deoxygenation had reached completion and to assure that the hemoglobin has reached a stable endpoint. During this work, Parkhurst *et. al.* showed that there was a dependence of apparent fractional saturation on wavelength, that is, fractional saturation is not exactly proportional to the absorbance change. All of the spectrophotometric studies before Parkhurst *et. al.* assumed that an absorbance change at a single wavelength can determine the four binding Adair constants. This assumption was challenged by Rifkind and Lumry, and Nasuda-Kouyama, but not widely accepted.[22,23] Parkhurst *et. al* focused on using multiple wavelengths in global fitting to determine the true Adair constants of hemoglobin binding to oxygen.

Chapter 2 ICAM Design & Calibration

2.1 Introduction

In previous spectrophotometric studies of hemoglobin equilibria, the protein needed to be in solution, and not inside of the cell. This was due to the turbidity of erythrocyte suspensions.[24] Scattering effects have always been a systematic problem in absorption measurements.[25] There have been various attempts to correct for the scattering. An example of one of these attempts is the Integrating Cavity Absorption Meter, or ICAM.

ICAMs and their derivatives use spectrophotometers that utilize multiple passes of light within the ICAM to increase the measured absorbance of a sample having a low concentration of absorbing particles.[26] The ICAM itself is a sphere with an entrance and exit window, with either the inner or outer diameter of the sphere coated with a highly diffuse reflecting white material. The walls reflect the light in a Lambertian manner until photons are either absorbed by the sample, or leaves through either the entrance or exit windows.[27] ICAMs have been used to study pollution detection or sea particles where the samples involved low extinction coefficients.[28,29]

Initial work on an ICAM began in 1953 when Walsh proposed that if light is introduced through a small entrance window, and the surface of the sphere was Lambertian reflective, then any point of reflectance in the ICAM will illuminate all other surfaces of the wall equally.[30] In 1970, Elterman continued the work by devising an integrating cavity and deriving the absorbance coefficients based upon the measured absorbances.[31] The derivations were based upon the energy of light at all points of the walls of the ICAM being equal. In 1992, Fry continued his work and continued to correct

Elterman's derivations.[32,33] The derivations use an average pathlength in the ICAM, derived from using the photon energy of light being equal at any one point of the ICAM.

Parkhurst derived the correct equations for both spherical and cubic ICAM to obtain absorbance coefficients from measured absorbance of the ICAM by considering the precise distribution of path lengths. Instead of considering the ICAM with average energy, Parkhurst integrated over the probabilities of all pathlengths within the ICAM. Using these unpublished results, Parkhurst found that the measured absorbance from an ICAM would follow an exponential complement with respect to absorbance per cm in the ICAM. The ICAM shape does matters, and the ICAM calculations could not follow a linear relationship.

Two designs of the ICAM were developed. The equations of the first design, denoted ICAM-milk, have been solved by Parkhurst. In ICAM-milk the sample is in solution and does not scatter.[34] The ICAM-milk will be used for non-light scattering samples to allow detection of low absorbance samples (*fig. 2.1 and 2.2*) . The second design, named ICAM+milk, cancels the Mie scattering of the erythrocytes by overwhelming it. By adding 1% by volume of 1% fat milk to the ICAM, the caseins and the fat globules both scatter the light more than the erythrocytes (*fig. 2.3*). The second design will focus on placing samples that scatter light in the ICAM+Milk. The final design of the ICAM is shown on figure 2.4, and details of the apparatus can be found in appendix A. Our initial task was to calibrate both ICAMs by comparing the measured absorbance from the ICAM to a scaled absorbance from the HPDA 8452 spectrophotometer of a sample that has no light scattering properties. Horse heart

metmyoglobin, the oxidized form of the myoglobin, was decided to be the sample for calibration. Metmyoglobin was chosen as the standard sample, as it absorbs across the visible spectrum, has 4 different peaks to ensure precision on the wavelength basis, and does not dissociate nor change its spectrum at a fixed pH.[35]

2.2 Materials and Methods

The initial ICAM design uses a 250 mL roundbottom flask with a sidearm, coated on the outside with a thick, even layer of white paint. A bright pen-light was inserted onto the open neck of the roundbottom flask in complete darkness to ensure nearly all light was contained except for escape through the two windows. The walls were diffusely reflecting and the light from the walls was isotropic Lambertian scattered. Two windows, without any paint, were directly across from one another. These two windows initially allowed the incident light to pass through the roundbottom flask. In the center top hole, a rubber stopper was crafted. In the center of the rubber stopper a cork borer (a shaft with a handle), which was surrounded by rubber on the top and by white waterproof paint on the bottom (*fig. 2.1*). At the bottom of the shaft a deflector was attached: a thin sheet of aluminum painted white, then lightly brushed with sandpaper. When the rubber stopper is placed into the top of the roundbottom flask, the rubber stopper with the cork borer attached deflects the incident light beam and causes the incident light to reflect onto the walls of the ICAM. When the rubber stopper was put into place, the initial reflection back through the entrance was eliminated. Effectively, an incident photon enters the ICAM through the entrance window, becomes scattered by the baffle, and reflects

multiple times in the ICAM until it leaves through the exit window, or it is absorbed within the ICAM by a sample. The light leaving the exit window is completely diffuse.

The final design of the ICAM encompassed a stable temperature control, measurement of the temperature of the solution inside of the ICAM, and measurement of the oxygen concentration (*fig 2.4*). A stable temperature was maintained by pumping water from a water bath through tygon tubing surrounding the ICAM. The tygon tubing was wrapped around the ICAM 15 times. A hole was made in the rubber stopper and a thermistor slid into place. Refer to figure 2.4 for the placement of these objects. The thermistor was connected to a voltmeter, and a calibration curve of voltage versus temperature from 15ºC to 40ºC was established. The temperature was held at room temperature for an hour within ±0.1 degrees. The sidearm contained an YSI 5300 oxygen electrode.[36] When placed into the sidearm, an airtight seal was made with silicone cement. The digital signal of the oxygen electrode was converted to analog using a Sparkfun Redboard microprocessor, and relayed to a computer through a mini-usb port.

After several experiments, it was determined that a special apparatus holder needed to be designed (*appendix A*). Our aims for the kinematic design were 1) to allow an air-powered stir plate to be introduced underneath the ICAM roundbottom flask, 2) allow adjustment of the ICAM for translation and rotation, and 3) to maintain the reproducible placement during removal and replacement of the ICAM.[37]

During our experimentation, two different set-ups of the ICAM instrument were used. Both utilized a baffle angled such that no incident light would pass through the

ICAM without reflecting off the walls of the ICAM. This setup was called "ICAM-milk." A second set-up of the ICAM was introduced, which included adding milk before the zeroing and baselining processes (*fig. 2.3*). The 1% fat milk at 1% by volume within the ICAM contains fat globules, roughly 3 μm in diameter at an average separation of 50 μm.[38,39] The fat globules strongly scatter light.[40] By introducing 1% (v/v) of 1% fat milk, which effectively scatters the light within the ICAM, the average photon would have a longer path length in the absence of absorption before exiting the ICAM. This setup was called "ICAM+milk."

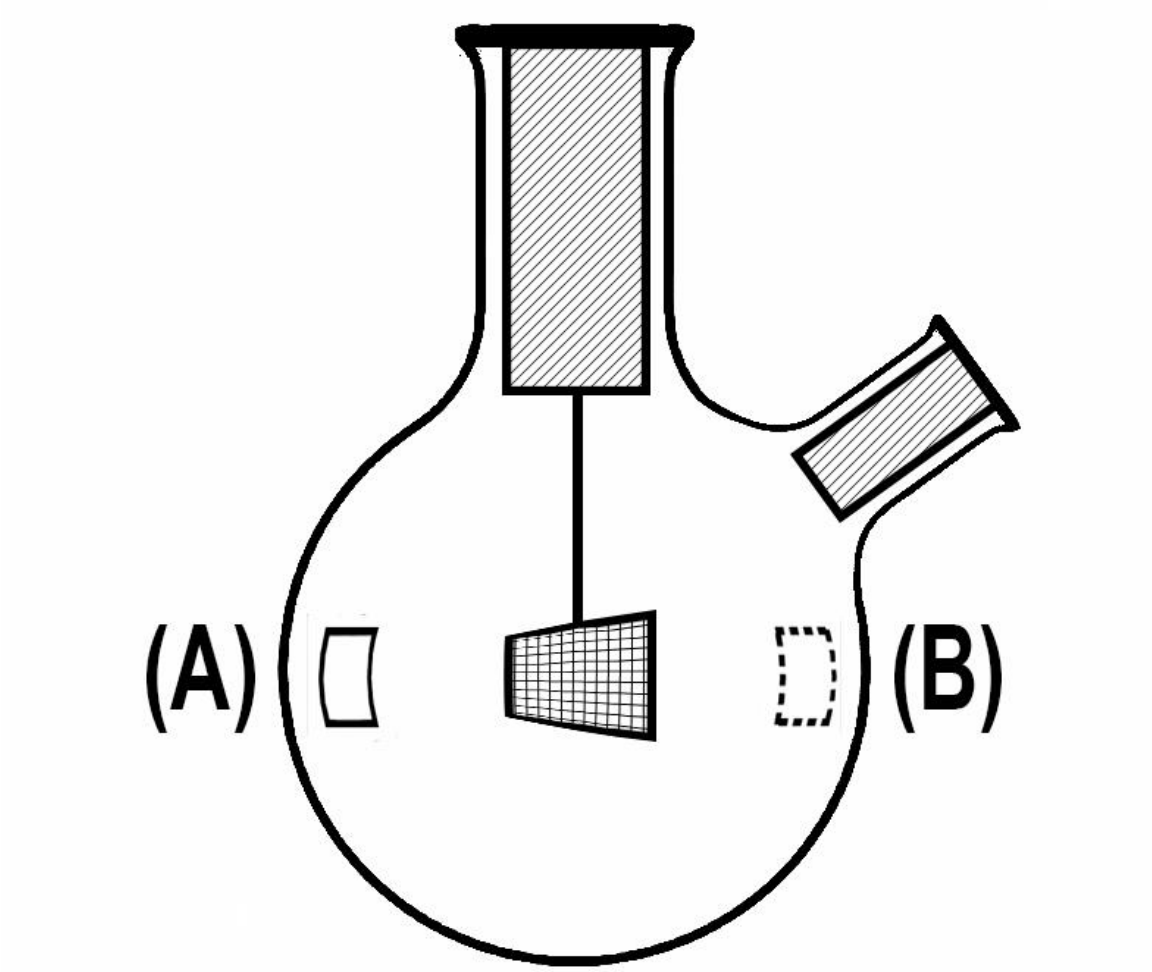

Figure 2.1: Model of the ICAM Design

A represents the entrance window for the incidence light, and *B* represents the exit window for the diffuse light. In between lies a white baffle secured using a white cork bore within a white rubber stopper. The sidearm was secured with a rubber stopper also painted white.

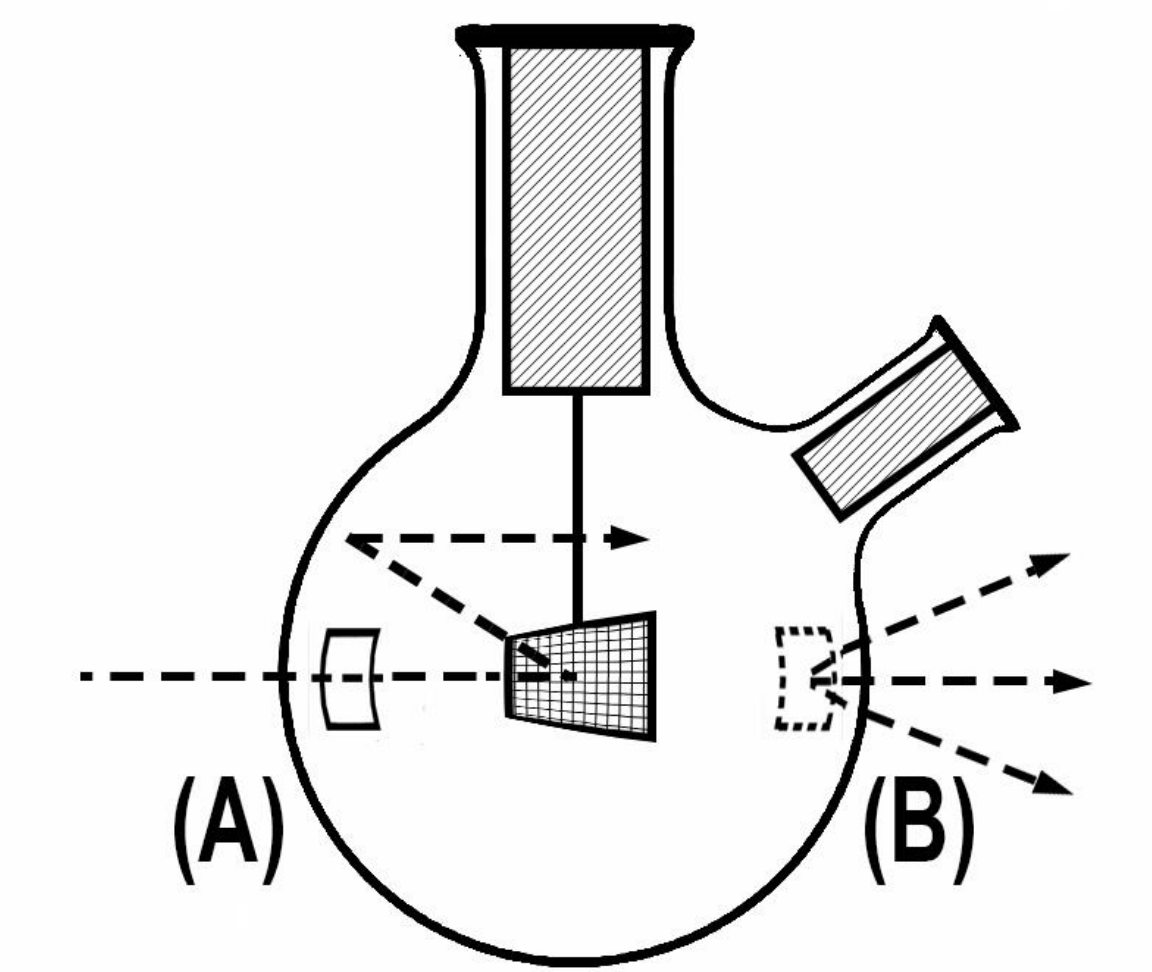

Figure 2.2: Model of the Light within the ICAM-Milk

As the collimated light from the incidence beam travels through the entrance window *A*, the beam is Lambertian scattered by the baffle. After Lambertian reflection from the walls through multiple passes, the scattered light leaves through the windows.

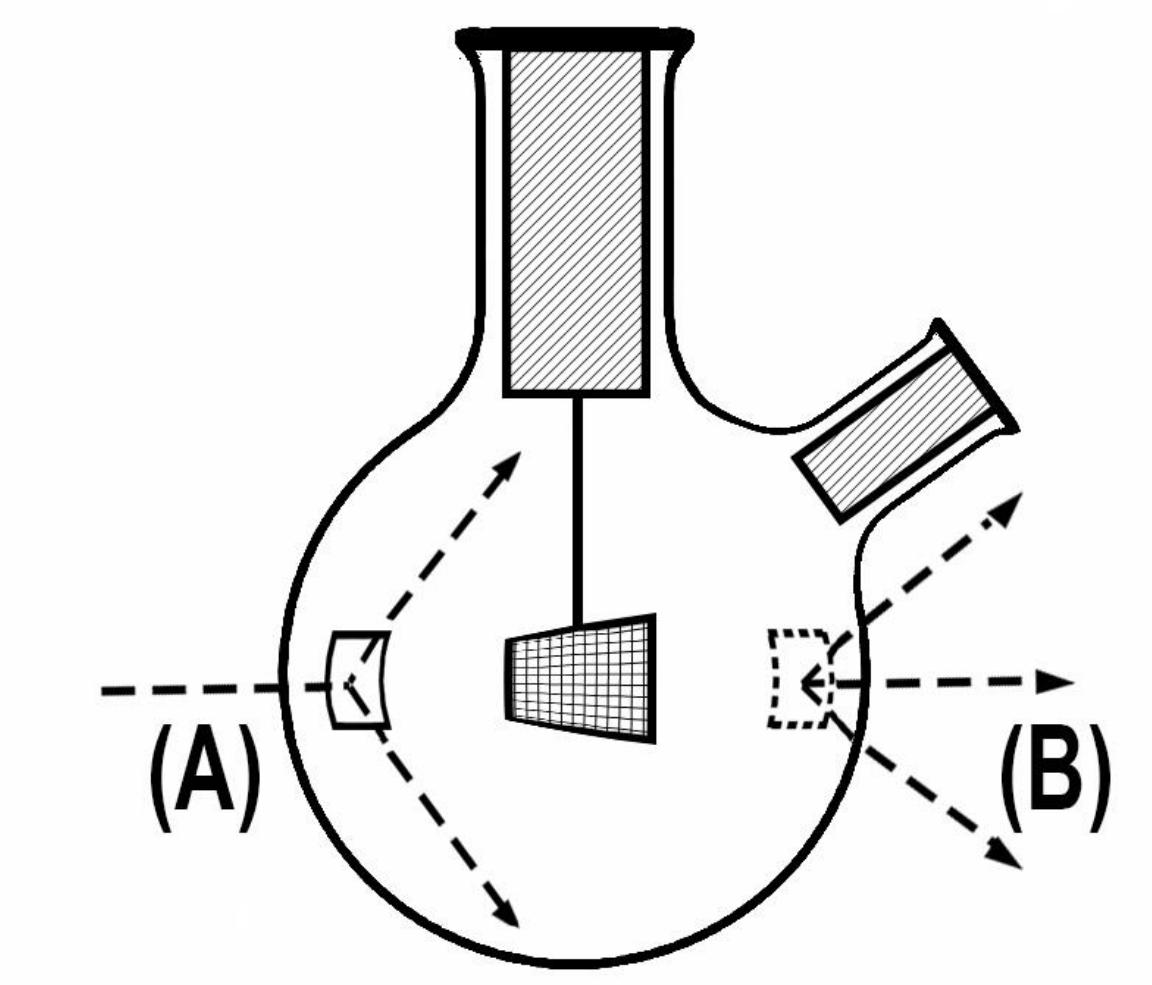

Figure 2.3: Model of the Light within the ICAM+Milk

As the collimated light from the incidence beam travels through the entrance window *A*, the beam is Lambertian scattered by the baffle and the milk particles. The light beam can be reflected multiple times by the milk before being reflected by a wall. After Lambertian reflection from the walls through multiple passes, the scattered light leaves through the windows.

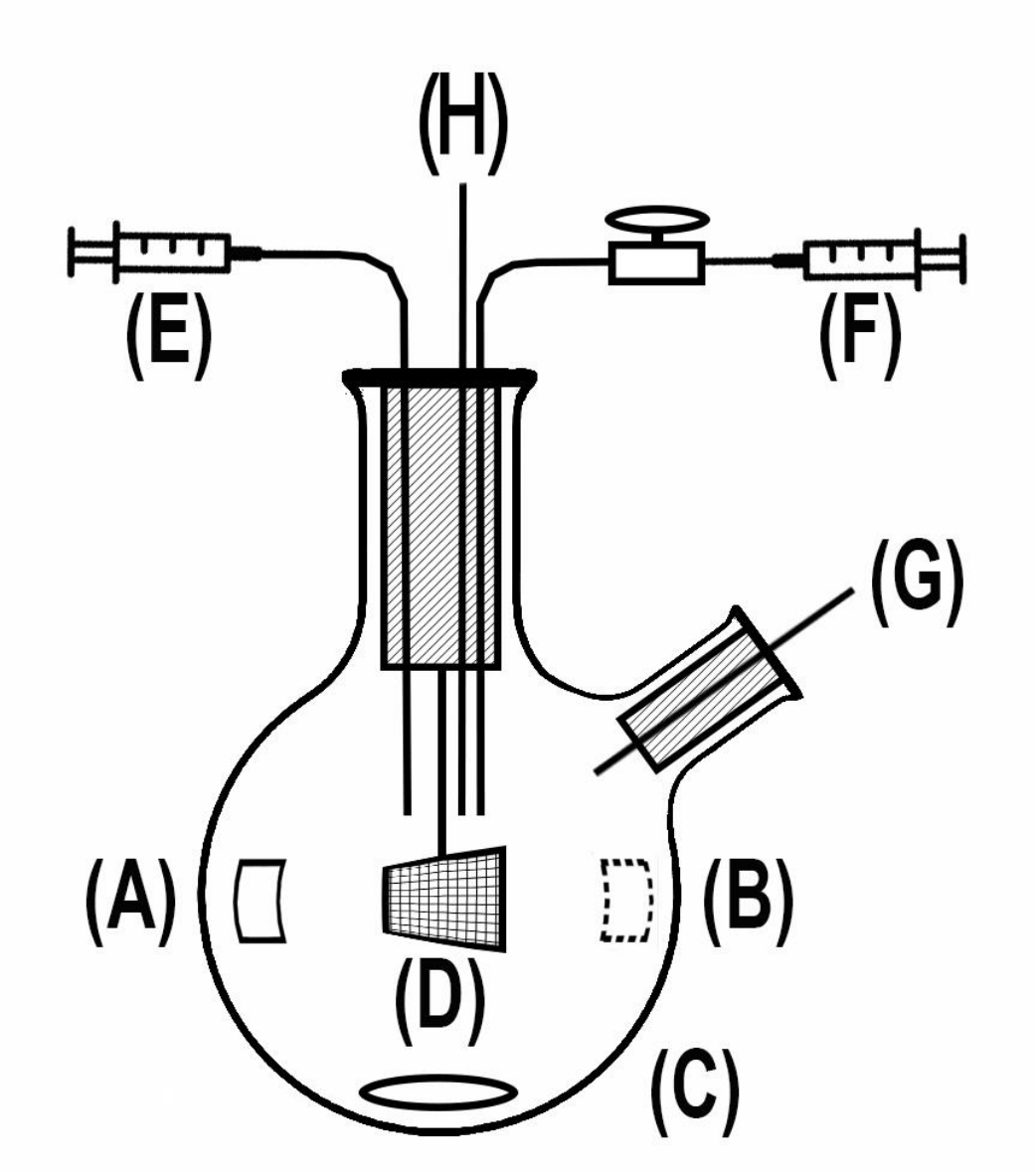

Figure 2.4: Model of the ICAM+Milk during the Deoxygenation of Erythrocytes

A represents the entrance window. *B* represents the exit window. *C* represents the stir bar, and *D* represents the baffle. *E* represents the overflow syringe, and *F* represents the enzyme syringe with an open-close valve. *G* represents the oxygen electrode. *H* represents the thermistor.

Calibration curves were constructed to test the relationship between the measured absorbance of metmyoglobin in solution in the ICAM versus the absorbance per centimeter of metmyoglobin in the HPDA 8452. Metmyoglobin (Mb^+), oxidized myoglobin, was chosen as the correcting sample, as it absorbs across the visible spectrum, and has 4 different absorption peaks at 500 nm, 542 nm, 575m, and 632 nm to ensure precision on the wavelength basis.[35]

A solution of metmyoglobin was prepared by adding 0.010 grams of potassium ferricyanide to 50 mL 50mM phosphate buffer, pH 8.0, with 1.2 grams of horse heart myoglobin. The ferricyanide separated from the Mb^+ with a G-25 Sephedex medium column. The column ran for 20 minutes and the metmyoglobin was collected, and well separated from the yellow ferricyanide. The concentration taken with the HPDA 8452 spectrophotometer, after a 1:20 dilution, using the molar extinction coefficient of $9.5*10^3$ $M^{-1} * cm^{-1}$ at 500 nm.[41] Using the HPDA 8452 spectrophotometer, a standard metmyoglobin spectrum from 500 nm-750nm was taken. Spectra of increasing concentrations of metmyoglobin were taken in the ICAM. A series of measured absorbance spectra in the ICAM+milk and the ICAM-milk were recorded and compared compared at each wavelength to the standard scaled absorbances from the standardized metmyoglobin spectra from the HPDA 8452. This plot was fitted well using an exponential complement function with an automated Monte-Carlo fitting program within Graphpad:[42]

(3) $$f(x) = A * (1 - e^{-B*x})$$

where *B* represents the exponential decay parameter. This function serves as a transfer function, allowing the measured absorbance of the ICAM to be directly compared to 1 cm pathlength HPDA spectra.

2.3 Results and Discussion

The standard spectrum of metmyoglobin (*fig. 2.5*) was scaled to the measured absorbances of the metmyoglobin in the ICAM-milk and the ICAM+milk (*fig. 2.6 and 2.8*) and compared (*fig. 2.7 and 2.9*). Both of the curves were well-fitted by exponential complements. These yielded the following transfer functions:

(4) $$y = 1.423 * (1 - e^{-9.937*x})$$

(5) $$y = 0.9375 * (1 - e^{-40.03*x})$$

for the ICAM-milk and the ICAM+milk, respectively, where *x* represents the absorbance per centimeter pathlength, and *y* represents the measured absorbance in the ICAM. The curve for the ICAM+milk showed much greater sensitivity for low absorbances as compared to the ICAM-milk (*fig 2.10*). In both systems, Lambertian reflection occurs at the walls of the ICAM, but the fat globules in the ICAM+milk gave much longer pathlength for photon absorption. which explains the higher resolution at lower concentrations.

The curve fit equations 4 and 5 represent operational equations of input-output. The input, x, for equations 4 and 5 represents the typical absorbance per centimeter pathlength, and the output represents the measured absorbance in the ICAM. Reversing

equation 3 gives equation 6, which uses the measured absorbance in the ICAM as the input, and the output is the typical absorbance per centimeter pathlength. This will yield a typical absorbance per cm from the highly non-linear ICAM measurements.

(6) $$x = -\frac{\ln(\frac{-y}{A}+1)}{B}$$

where *x* represents the measured absorbance in the ICAM, and *A* and *B* represent the same parameters from equations 3, 4, and 5. The inversed transfer functions for the ICAM-milk and the ICAM+milk are respectively:

(7) $$x = -\frac{\ln(\frac{-y}{1.423}+1)}{9.937}$$

(8) $$x = -\frac{\ln(\frac{-y}{0.9375}+1)}{40.03}$$

where *x* represents the measured absorbance in the ICAM, and *y* represents typical absorbance per centimeter.

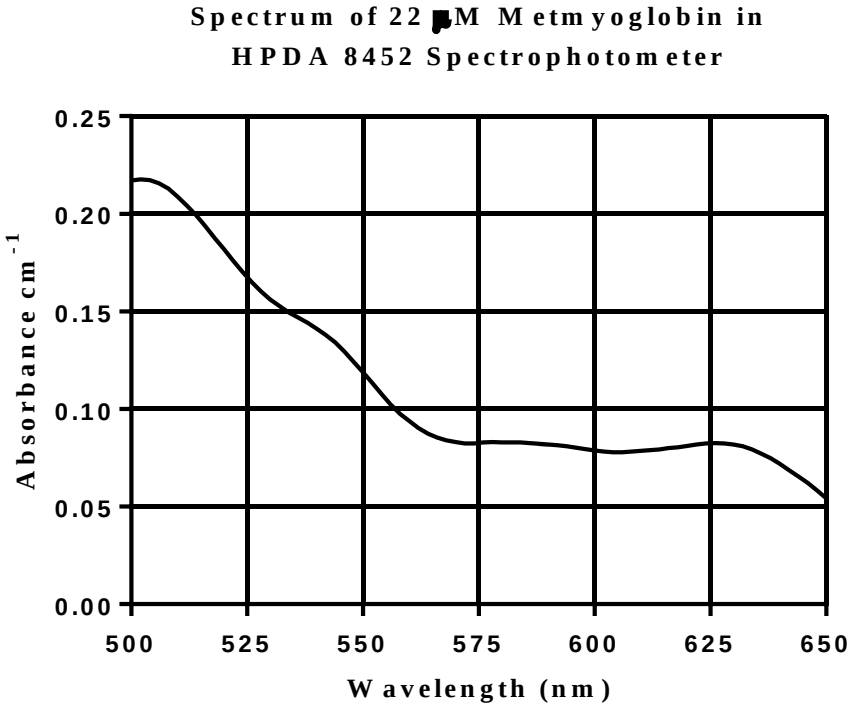

Figure 2.5: Standard Spectrum of 22 µM Metmyoglobin

The standard spectrum of metmyoglobin in a HPDA 8452 spectrophotometer was obtained by taking 10 scans ($\Delta\lambda$=2 nm) smoothed using a 9-window quadratic Savitsky-Golay filter, then averaged.

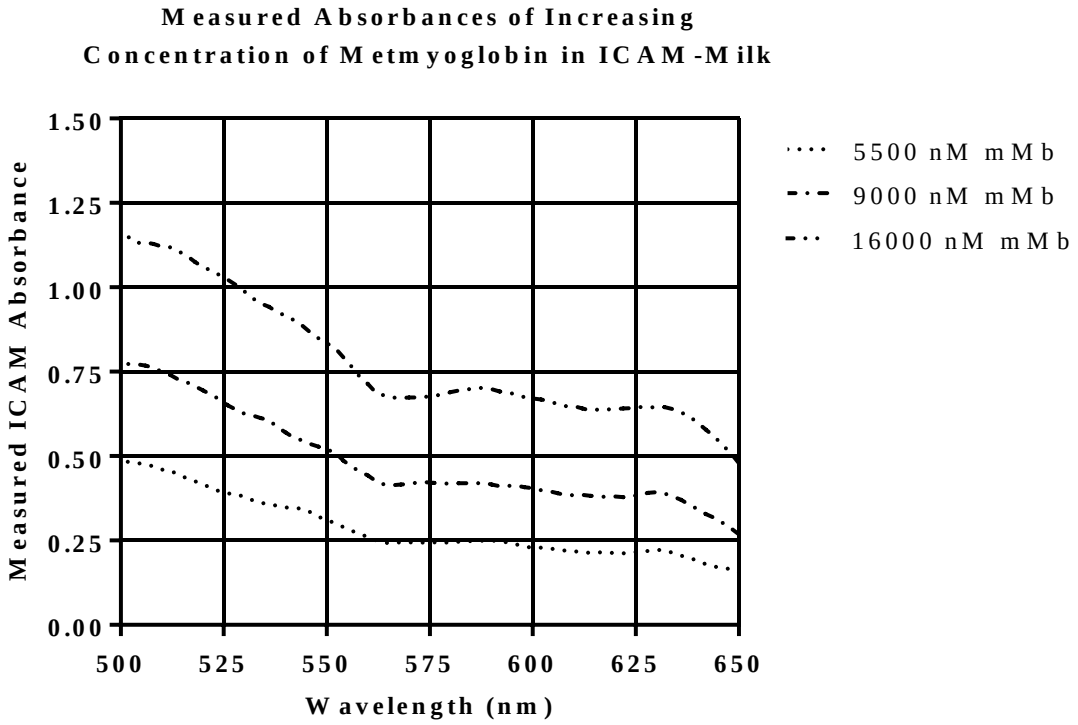

Figure 2.6: Measured Absorbances of Metmyoglobin in the ICAM-Milk.

A series of increasing concentrations of metmyoglobin in the ICAM-milk had 10 spectral scans for each concentration smoothed using a 9-window Savitsky-Golay filter, then averaged. The dilutions were from 31 nM, 110 nM, 270 nM, 620 nM, 1300 nM, 2400 nM, 3800 nM, 5500 nM, 9000 nM, and 16000 nM, metmyoglobin. Shown here are the curves from 5500-16000 nM are shown.

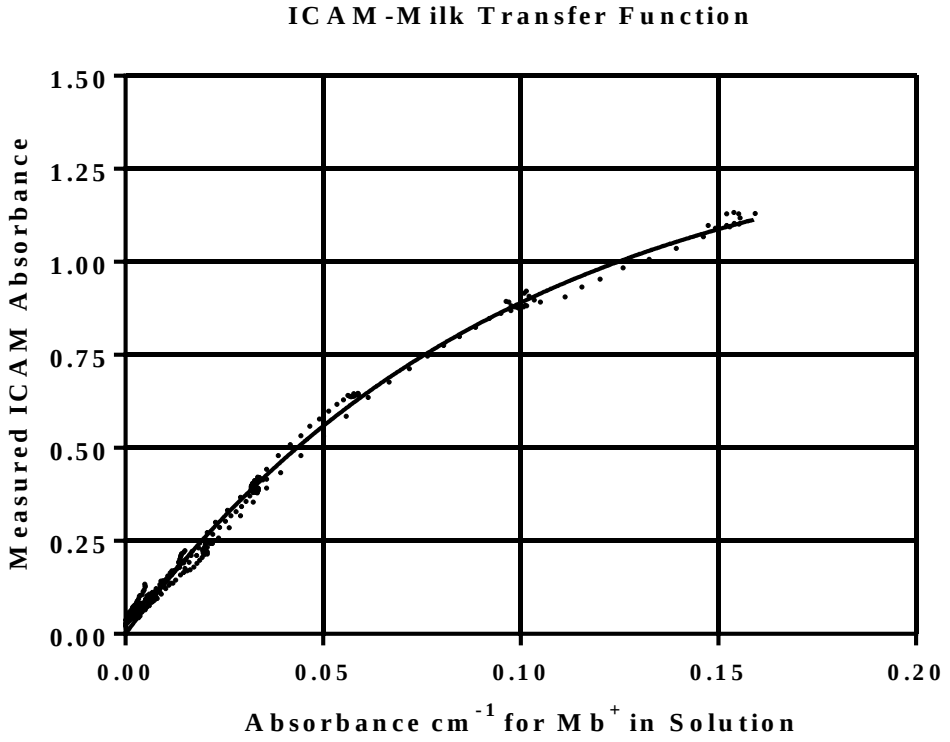

Figure 2.7: ICAM-Milk Transfer Function

For any particular wavelength, the measured absorbances from the ICAM were plotted on the *y*-axis, whereas absorbance cm^{-1} data were plotted on the *x*-axis (*see fig. 2.5 and 2.6*). The 756 data points plotted on this curve for metmyoglobin ranged from 500 to 650 nm. The data were well-fitted by an exponential complement $f(x) = A * (1 - e^{-B*x})$, where A equals 1.423 ± 0.036, and B equals 9.937 ± 0.376. $\sigma_{fit} = 0.02775$

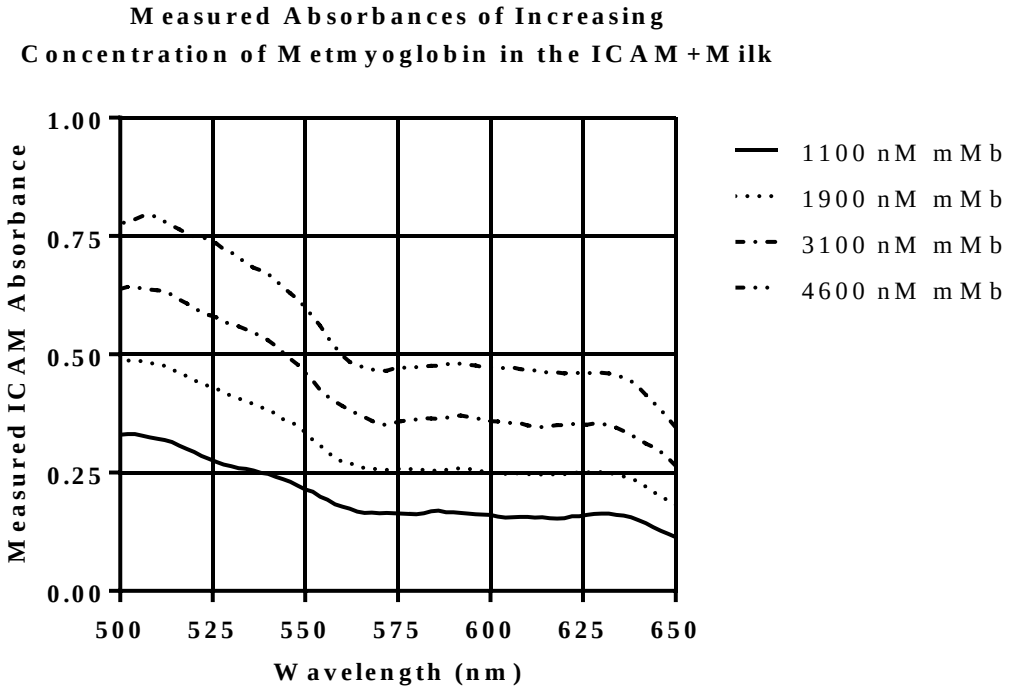

Figure 2.8: Measured Absorbances of Metmyoglobin in the ICAM+Milk

A series of increasing concentrations of metmyoglobin in the ICAM+milk had 10 spectral scans for each concentration smoothed using a 9-window Savitsky-Golay filter, then averaged. The dilutions were 29 nM, 88 nM, 220 nM, 510 nM, 1100 nM, 1900 nM, 3100 nM, and 4600 nM, metmyoglobin.

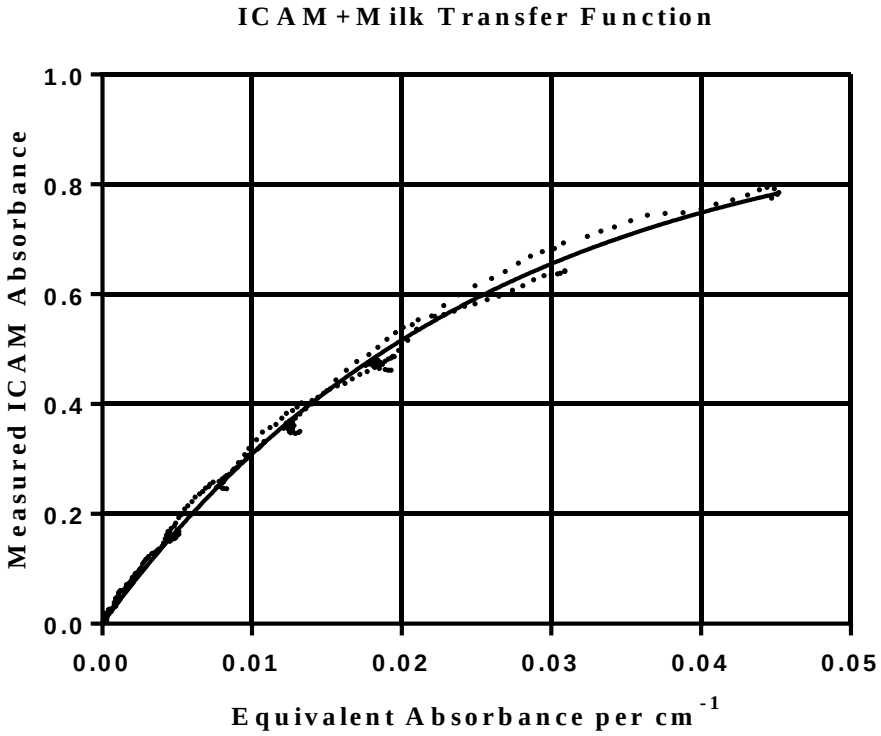

Figure 2.9: ICAM+Milk Transfer Function

For any particular wavelength, the measured absorbances from the ICAM were plotted on the *y*-axis, whereas absorbance cm^{-1} data were plotted on the *x*-axis (*see fig. 2.7 and 2.8*). The 600 data points plotted on this curve for metmyoglobin ranged from 500 to 650 nm. The data were well-fitted by an exponential complement $f(x) = A * (1 - e^{-B*x})$, where A equals 0.9375 ± 0.006917, and B equals 40.03 ± 0.4584. $\sigma_{fit} = 0.01193$

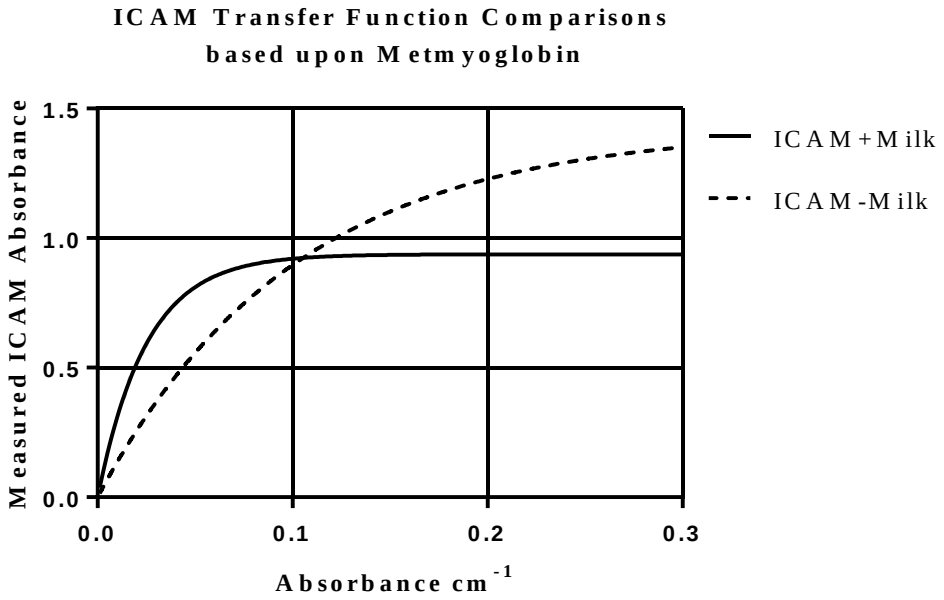

Figure 2.10: ICAM Transfer Function Comparisons

Shown are the two transfer functions from figures 2.7 and 2.9.

Chapter 3 Validation of the ICAM Transfer Functions

3.1 Introduction

Metmyoglobin (Mb^+) was used to establish the transfer functions that related non-linear measured absorbances from the ICAM to the absorbance per centimeter of the Mb^+ solution within the ICAM. The ICAM+milk transfer function is appropriate for both turbid and non-turbid samples in the presence of the turbid milk. As a control, the spectrum of hemoglobin within the erythrocyte was determined independently of the ICAM using thin-layers of packed non-scattering erythrocytes (*fig 3.4*) in the HPDA 8452 spectrophotometer. This technique was used by Professor Parkhurst for crystals of erythrocytes containing carbon monoxide in 1967.[43] The measured absorbance of hemoglobin within the erythrocyte in the ICAM+milk was transformed into absorbance per centimeter using the inverse transfer function (*fig 3.5 & 3.6*). The absorbances per centimeter of the suspension of erythrocytes in the ICAM+milk were compared to the absorbances of thin-layer of packed erythrocytes (*fig. 3.7*). This comparison showed that the transfer function correctly provides the spectrum of the oxyhemoglobin within the erythrocyte for erythrocytes in suspension in the ICAM+milk.

The ICAM-milk transfer function was meant for non-scattering samples. The measured absorbances of hemoglobin in solution in the ICAM-milk were transformed to absorbance per centimeter using the inverse transfer function (*fig. 3.1 & 3.2*). The absorbances per centimeter of hemoglobin in solution in the ICAM were compared to absorbances of hemoglobin in solution in the HPDA 8452 spectrophotometer (*fig. 3.3*). This validates the procedure.

3.2 Materials and Methods

Erythrocytes from Professor Parkhurst were collected into citrate tubes at the UNL Health Center and on the same day were centrifuged at 1000xg for 3 minutes and the supernatant replaced with 1% (w/v) sodium chloride in 50mM phosphate buffer, pH 6.8. Continued centrifugation and washing occurred until the supernatant was clear. Hemoglobin from such samples was prepared by lysing the cells with a three times excess of deionized H_2O, centrifuging the sample at 1000xg, and collecting the supernatant. Spectrophotometric studies of hemoglobin were at concentrations above 150 µM in heme to avoid dissociation of the tetramer.[44,45] Long-term storage at 4ºC and at -80ºC are discussed in appendix D. The suspensions of erythrocytes were centrifuged at 2000x*g* for 20 minutes, and the supernatant removed. The erythrocytes (50 µL) were placed on a microscope slide using a modified glass pipette with a larger diameter at its tip. A cover slip was gently placed on the packed erythrocytes. Using mild pressure and rubbing the cover slip resulted in the packed erythrocytes forming a non-scattering erythrocyte layer between 20 µm-30 µm in thickness. The thin packed erythrocyte layer was placed in the incident beam of the HPDA 8452, and the spectrum of hemoglobin within the erythrocyte taken. The ICAM+milk was blanked with 270 mL of 1% (w/v) NaCl 50mM phosphate pH 6.8 buffer with 2.7 mL of 1% milk. Afterwards, 600 µL of an erythrocyte suspension at 10% hematocrit was added to the ICAM and the spectrum was taken. The ICAM+milk measured absorbance was inverted to absorbance per centimeter using the inverse transfer function. The spectrum of hemoglobin within the erythrocyte in the thin layer and the spectrum of the ICAM+milk absorbance per centimeter were normalized to 576 nm and compared.

3.3 Results and Discussion

The transfer function approach used metmyoglobin for convenience. The spectrum of oxyhemoglobin, the sample that did not scatter light, was measured using the HPDA 8452. The measurement of oxyhemoglobin in the ICAM-milk, after inverse transformation (*eq. 7*) showed no differences between the two spectra. The ICAM+milk measured absorbance spectrum of hemoglobin within the erythrocyte were similarly transformed to equivalent absorbance per centimeter (*eq. 8*) and compared to the thin-layer spectrum. There were insignificant differences between the two spectra. Comparison of the spectra of the oxyhemoglobin within the erythrocyte to that of hemoglobin in solution showed differences (*fig. 3.8 and 3.9*). The spectrum of deoxygenated erythrocytes was compared to the literature values for deoxyhemoglobin, and a difference appears (*fig. 3.10*).[46] This is the first data showing the spectra of oxyhemoglobin and deoxyhemoglobin within the erythrocyte.

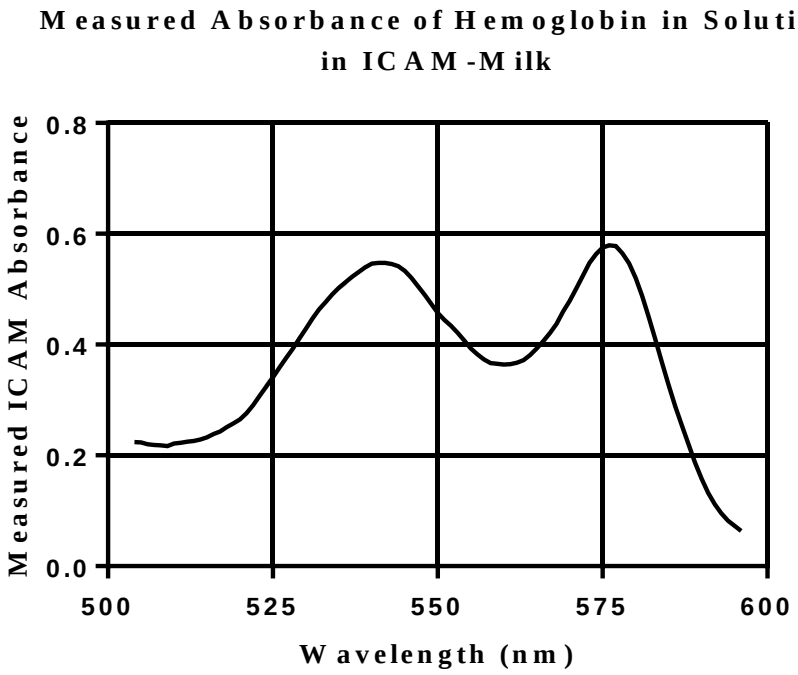

Figure 3.1: Measured Absorbance of Hemoglobin in Solution in ICAM-Milk

The measured absorbances of the hemoglobin in solution from the ICAM-milk were transformed to standard 1 cm pathlength absorbances using the inverse of the ICAM-milk transfer function, $x = -\frac{\ln(\frac{-y}{1.423}+1)}{9.937}$ (*eq. 7*).

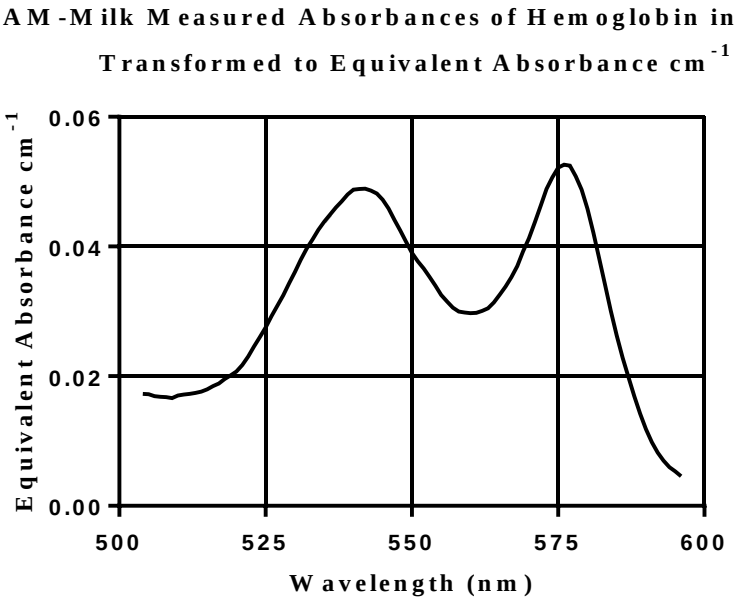

Figure 3.2: Absorbances of Hemoglobin in Solution in the ICAM-Milk Transformed to Equivalent Absorbance cm^{-1}

The measured absorbances (*fig. 3.1)* of the hemoglobin in solution from the ICAM-milk were transformed to standard 1 cm pathlength absorbances using the inverse of the ICAM-milk transfer function, $\boldsymbol{x = -\frac{\ln(\frac{-y}{1.423}+1)}{9.937}}$ (*eq. 7*), where *y* represents the measured absorbance and *x* represents the equivalent absorbance cm^{-1}.

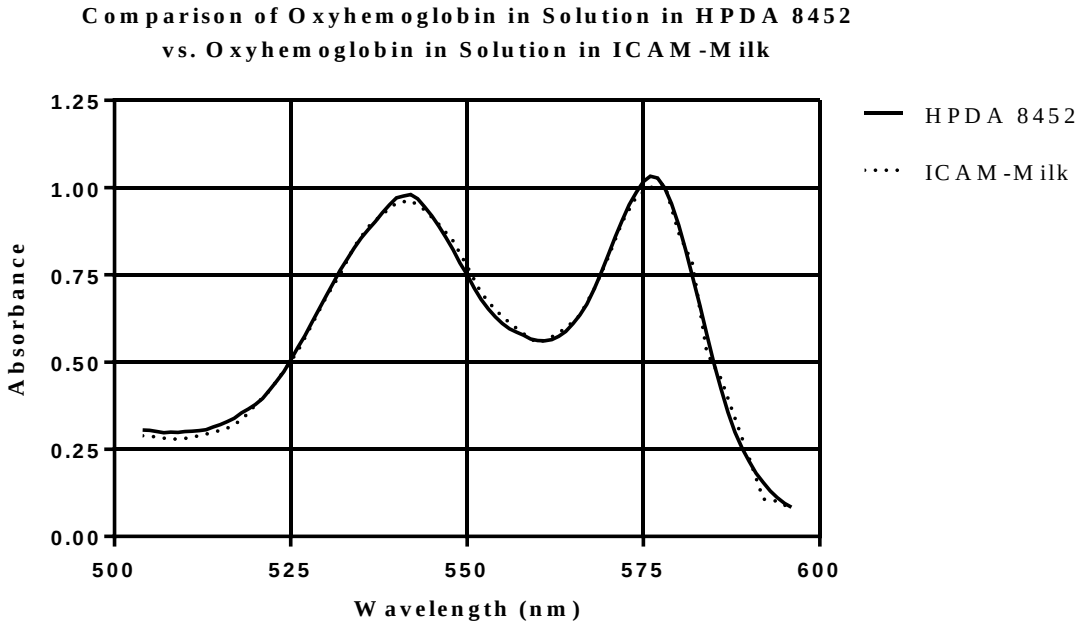

Figure 3.3: Comparison of Oxyhemoglobin in Solution using HPDA 8452 and ICAM-Milk

The spectrum from figure 3.2 was scaled and compared to the spectrum of hemoglobin in a one centimeter cuvette in the HPDA 8452. This shows that the ICAM-milk transfer function will allow us to transfer measured ICAM absorbances to true equivalent absorbance cm^{-1}.

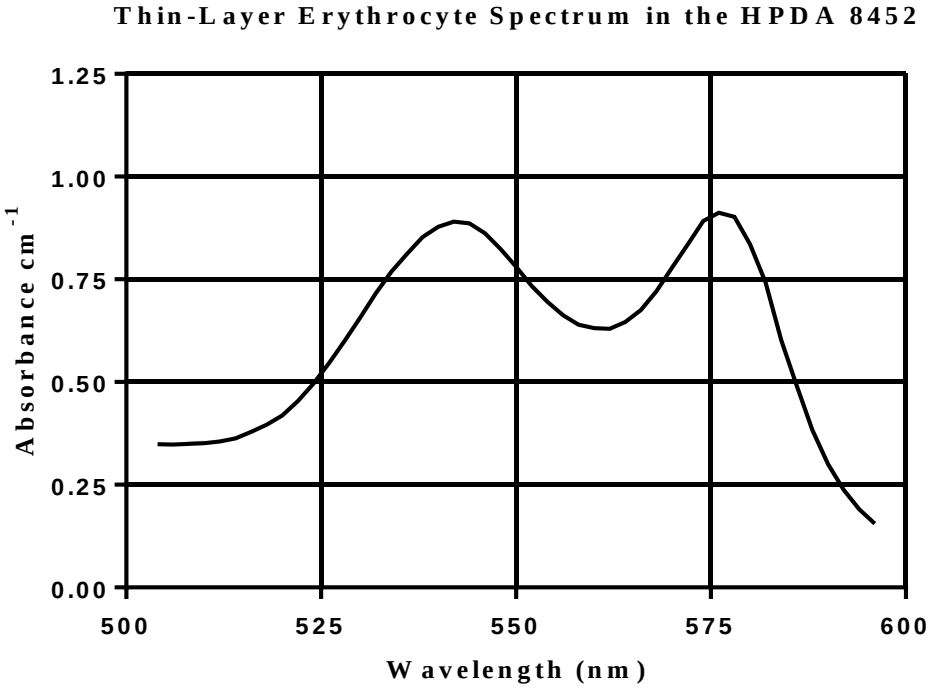

Figure 3.4: Thin-Layer Erythrocyte Spectrum in the HPDA 8452

Packed erythrocytes with the scattering-effects eliminated were placed in the incident beam of the HPDA 8452, and the spectrum was taken. No scattering effects were observed since there were no refractive index differences through the illuminated area of the sample.

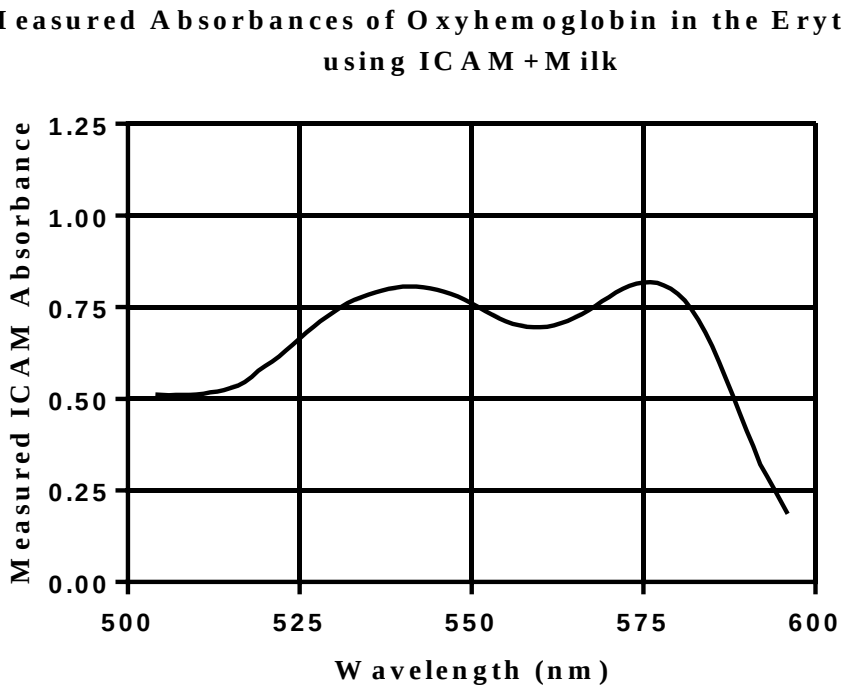

Figure 3.5: Measured Absorbances of Oxyhemoglobin within the Erythrocyte using ICAM+Milk

The measured absorbances of the hemoglobin in solution from the ICAM+milk were transformed to standard 1 cm pathlength absorbances using the inverse of the ICAM+milk transfer function, $\boldsymbol{x = -\frac{\ln(\frac{-y}{0.9375}+1)}{40.03}}$ (*eq. 8*), where *y* represents the measured absorbance and *x* represent the equivalent absorbance cm^{-1}.

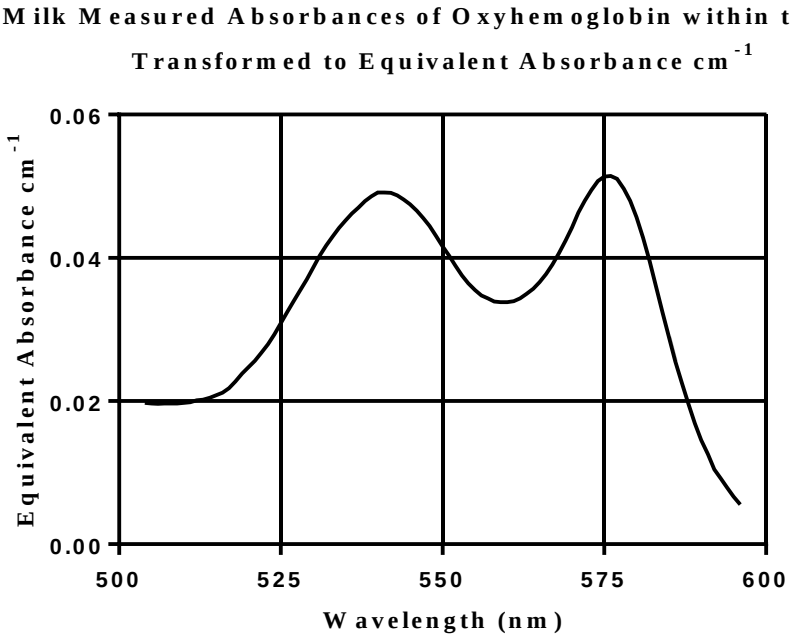

Figure 3.6: ICAM+Milk Measured Absorbances of Oxyhemoglobin within the Erythrocyte Transformed to Equivalent Absorbance cm^{-1}

The measured absorbances of the hemoglobin in solution from the ICAM+milk were transformed to standard 1 cm pathlength absorbances using the inverse of the ICAM+milk transfer function, $\boldsymbol{x = -\frac{\ln(\frac{-y}{0.9375}+1)}{40.03}}$ (*eq. 8*), where *y* represents the measured absorbance and *x* represent the equivalent absorbance cm^{-1}.

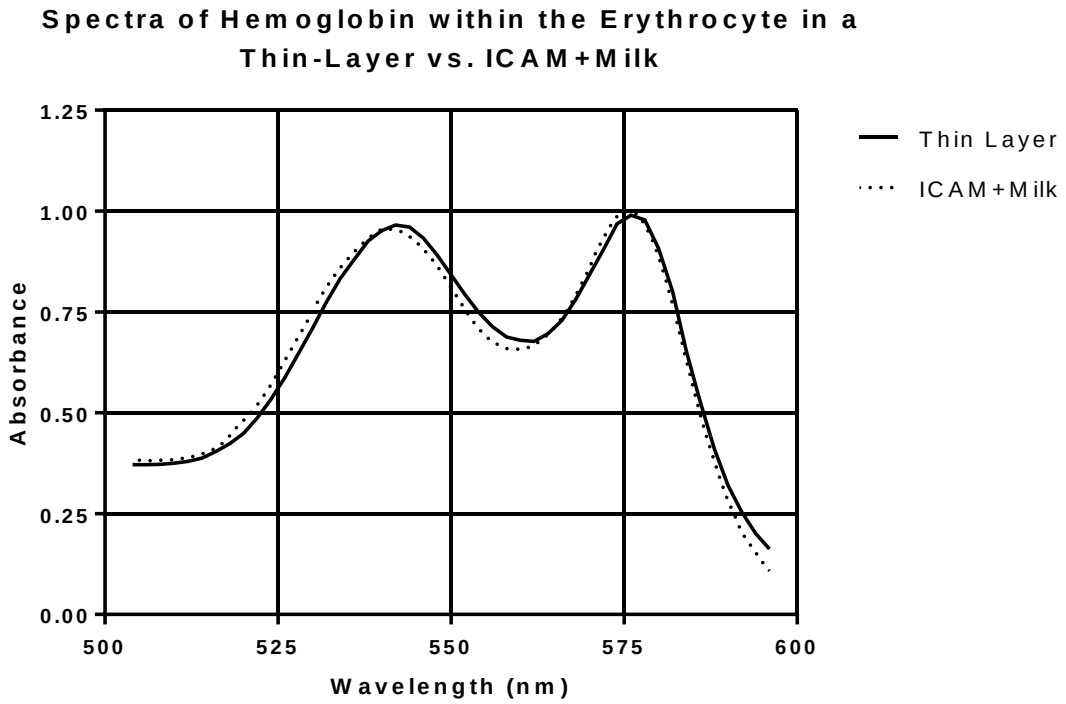

Figure 3.7: **Spectra of Hemoglobin within the Erythrocyte in Thin-Layer vs. ICAM+Milk**

The absorbance cm^{-1} obtained of hemoglobin within the erythrocyte using ICAM+milk and in the thin-layer were scaled and compared. This shows that the inverse transfer function will transform correctly measured absorbances of turbid samples to equivalent absorbance cm^{-1}, correctly eliminating scattering artifacts.

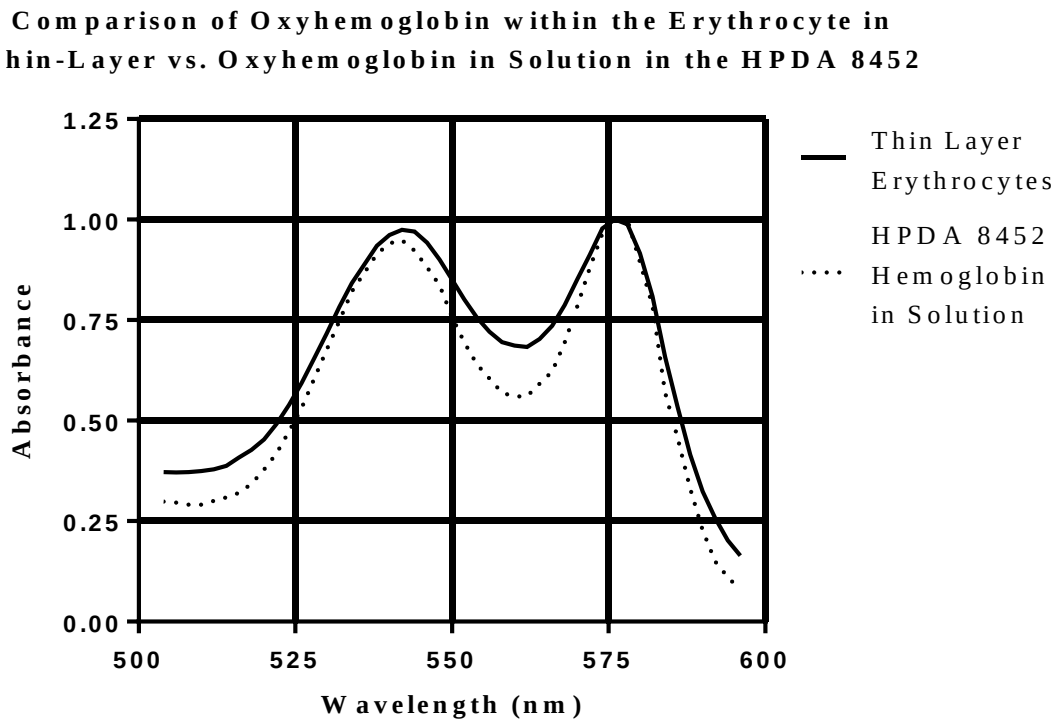

Figure 3.8: Comparison of Hemoglobin within the Erythrocyte in Thin-Layer vs. Hemoglobin in Solution in HPDA 8452

Optical differences between oxyhemoglobin within the erythrocyte versus oxyhemoglobin in solution are shown here, independent of the ICAM measurements.

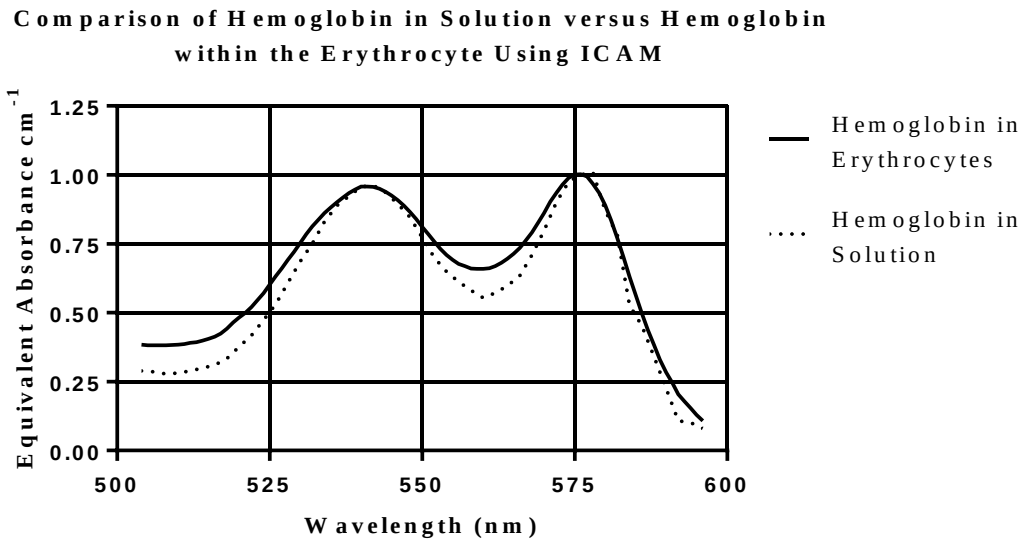

Figure 3.9: Comparison of Spectra of Oxyhemoglobin in Solution versus Oxyhemoglobin within the Erythrocyte Using ICAM

The optical differences between oxyhemoglobin within the erythrocyte measured with the ICAM+milk and oxyhemoglobin in solution are within error the same via figure 3.8 using the thin-layer method.

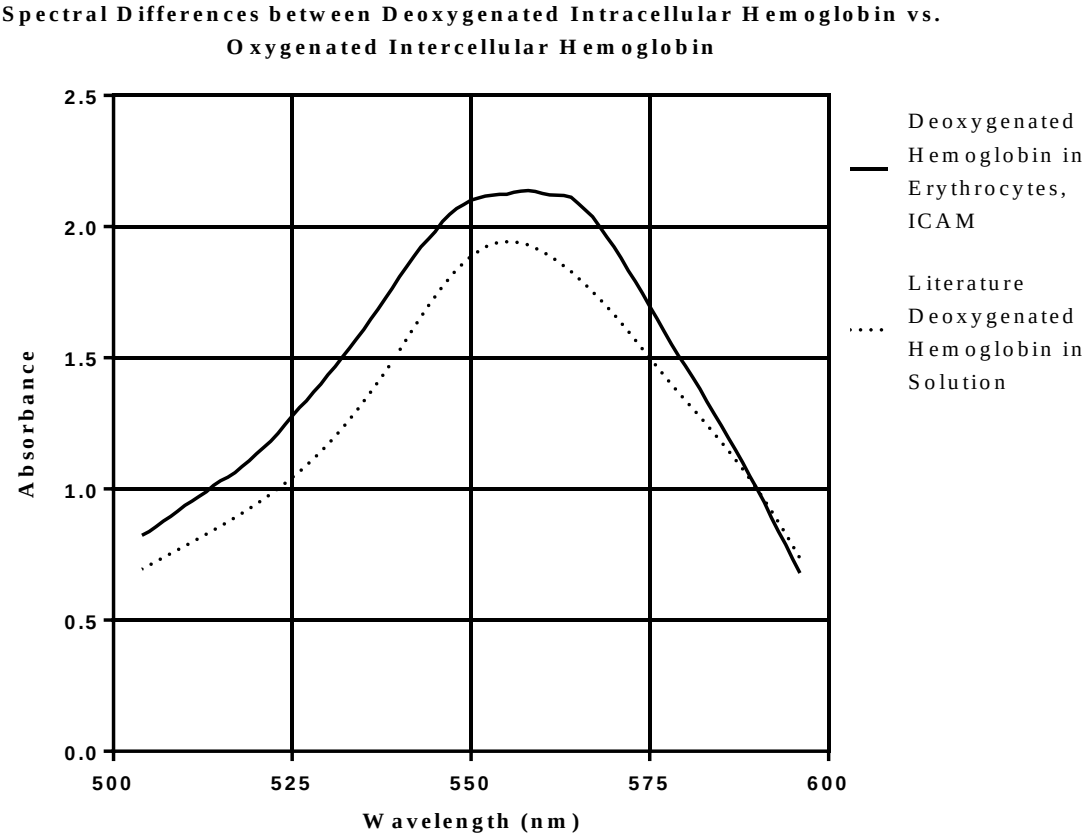

Figure 3.10: Spectral Differences between Deoxygenated Hemoglobin in Solution and within the Erythrocyte

Deoxygenated hemoglobin in erythrocytes (ICAM+milk) were compared to literature values by normalizing both to 590 nm.[46]

Chapter 4 Oxygen Binding in Intracellular Hemoglobin

4.1 Introduction

The previous chapter discussed spectral differences between hemoglobin within erythrocytes and hemoglobin in solution in both in the oxy- and deoxy- forms. This chapter will discuss preliminary oxygen binding data for erythrocytes using ICAM spectrophotometry. The oxygen binding curve will be used to determine the Adair constants and compared to data at the same wavelength for hemoglobin in solution.[19] The binding constants for oxygen to hemoglobin were obtained from the fractional saturation of hemoglobin as a function of the concentration of oxygen. The fractional saturation of hemoglobin, $\bar{Y}$, is the number of bound oxygen ligands, divided by four. The fractional saturation will be compared to the oxygen concentration.

(9) $$\bar{Y} = \frac{[bound\ sites]}{[bound\ sites]+[unbound\ sites]}$$

The ligand binding curve near $\bar{Y} = 0.5$ can be presented by means of the Hill plot.[47]

(10) $$\log\frac{\bar{Y}}{(1-\bar{Y})} = n_H * \log[x]$$

Where *[x]* represents the concentration of the ligand and n_H is the Hill number. The Hill number provides a measure of the cooperativity of the multi-ligand binding site protein. For n_H <1, the protein exhibits negative cooperativity; and for n_H >1, the protein exhibits positive cooperativity. The Hill equation can be used to find the half-saturation of the erythrocytes ($\bar{X}$), where $\bar{X}$ represents the oxygen concentration when half of the oxygen-binding sites of the hemoglobin are bound with oxygen. In 1925, Adair studied oxygen

binding to hemoglobin and found that the Hill plot for hemoglobin was not linear over the entire concentration range of oxygen. He found that four binding constants described the oxygenation of hemoglobin.[11] Adair used the four binding constants as phenomenological macroscopic constants, independent of any detailed model, provided the hemoglobin tetramer does not dissociate.

(1) $$\bar{Y} = \frac{1}{4} * \frac{K_I[x]+2K_1K_2[x]^2+3K_1K_2K_3[x]^3+4K_1K_2K_3K_4[x]^4}{1+K_1[x]+K_1K_2[x]^2+K_1K_2K_3[x]^3+K_1K_2K_3K_4[x]^4}$$

4.2 Materials and Methods

The ICAM+milk was used to measure the deoxygenation of hemoglobin within the erythrocytes. The ICAM needs to maintain a stable temperature, have a way to measure the temperature of the solution inside of the ICAM, have a system to measure the oxygen concentration, and a system to deoxygenate the sample (*fig. 4.1*). The temperature of the solution was monitored through a thermistor held in place by the rubber stopper (*fig. 2.4*). The thermistor was attached to a multimeter. The thermistor was calibrated with a calibration curve of voltage vs. temperature from 15ºC to 40ºC. The solution temperature in the ICAM was equilibrated in lab air. The solution temperature in the ICAM was checked over the course of one hour, with a range from 22 ± 0.1 ºC. The oxygen concentration was monitored using a Yellow Springs Instruments 5300 oxygen electrode (*appendix C*). The correct air pressure in the lab was 698 mmHg (*appendix E*). Both the temperature and the correct air pressure in the lab were used to determine the oxygen concentration in 100% air-equilibrated solution, which was 250 µM.

The deoxygenation of the sample employed ascorbic acid in combination with L-ascorbate oxidase from *Cucurbita sp.* obtained from Sigma-Aldrich. One unit of the ascorbate oxidase oxidized one µmole of *L*-ascorbate to dehydroascorbate per minute at pH 5.6 at 25ºC. The ascorbate oxidase from Sigma had 0.250 milligrams of ascorbate oxidase per unit. The oxidation of ascorbic acid to dehydroascorbate occurs in a four-electron reduction of oxygen to water without the production of free radicals. The ascorbate oxidase contains three moles of copper. The two copper centers in ascorbate

oxidase store reducing equivalents of from the ascorbate oxidase. This is confirmed by EPR signals consistent with the presence of free-radicals. The two copper centers are known to consist of a single type I copper site and a trinuclear copper, in which three coppers are separated by 12 Å to 15 Å from the single type I copper site.[48] It was found that the two copper sites interact separately with the two substrates, and that the free-radicals were contained within the enzyme and do not produce hydrogen peroxide.[49] This removed the possibility of free-radicals forming during the deoxygenation of the erythrocytes from enzymatic action.

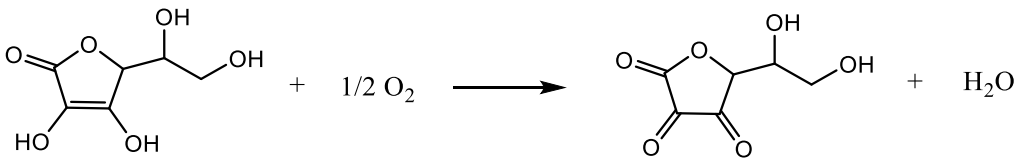

The ICAM+milk had a total volume of 272 mL, consisting of 260 mL of 1% (w/v) sodium chloride, 50 mM phosphate buffer, pH 6.8 with the addition of 10 mL of 2.6 M ascorbic acid, and 2.76 mL of 1% milk. A syringe of 25 U of ascorbic acid was prepared in 1 mL 1% (w/v) NaCl, 50 mM phosphate buffer, pH 6.8. The tubing leading into the ICAM had a valve for enzyme delivery (*fig. 2.4*). A second empty syringe was also placed in the ICAM to capture overflow (*appendix B*). The dead time of enzyme mixing was measured to one second. At time zero, the enzyme was injected, and the valve promptly closed. The ICAM milk system scanned every nanometer from 600 to 500 nanometers with a signal averaging of 66 milliseconds. The spectral bandwidth was set to 0.6 nanometers to ensure adequate signal-to-noise ratios. The monochromator scanned from 600 to 500 nanometers in 12 seconds, then slewed back to 600 nanometers

in 3 seconds. During the slew time, no data was recorded. A reading at the same wavelength occurred every 15 seconds. The oxygen depletion was measured using the oxygen electrode. After 8 minutes of unchanged absorbance readings, 1 mL of 0.57 M sodium dithionite was injected to ensure complete deoxygenation.

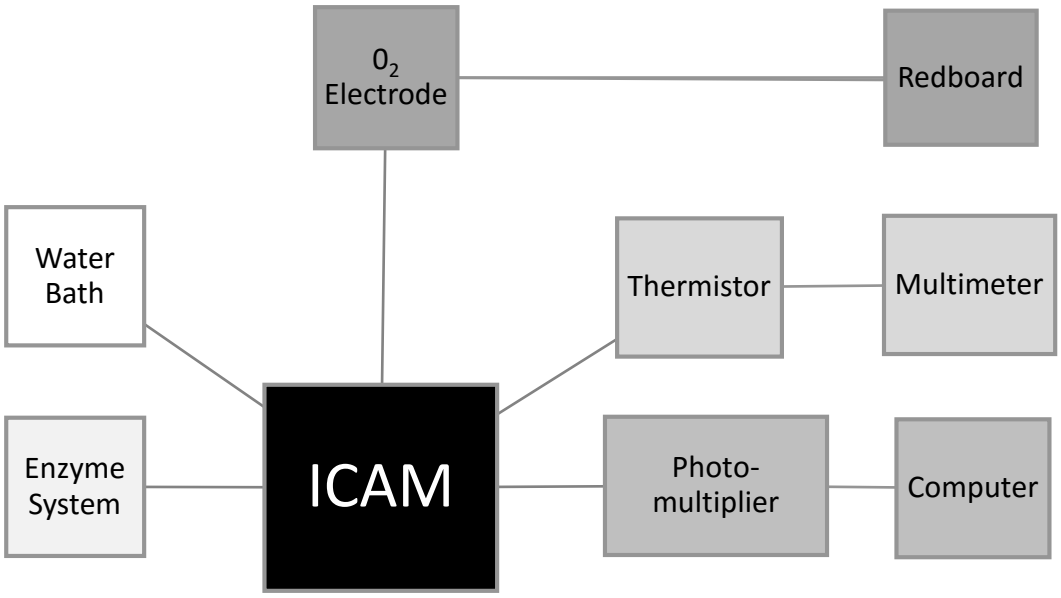

Figure 4.1: Block Diagram of the Instrumentation

The ICAM system employed a Cary 300 to measure spectra from light-scattering sources. The temperature is monitored by a thermistor inside the ICAM and the signal is monitored by a multimeter. The O_2 concentration is monitored by a Yellow Springs Instruments 5300 oxygen electrode *(appendix C)*. Circulating water from a water bath can be used to set the temperature.

4.3 Results and Discussion

Preliminary workup of the oxygen binding data for erythrocytes used 576 nm absorbances. The gradual loss of absorbance at 576 nm both from the measured ICAM absorbance and the equivalent absorbance cm^{-1} is depicted in figures 4.3 and 4.4. The voltage of the oxygen electrode (*fig 4.2*) was set to 5 V with air-equilibrated water, corresponding to air-equilibrated water at a concentration of 250 µM O_2 (*appendix E*). The voltage vs. time was fit to a curve fit of:

(11) $$Voltage = (1.781 * 10^{-12}x^4) - (9.79 * 10^{-9}x^3) + (1.933 * 10^{-5}x^2) - (0.01634x) + 5.096$$

(12) $$[O_2] = \frac{Voltage}{5} * [O_2]\ in\ air - equilibrated\ water$$

where *x* represents the time in seconds. The voltage divided by 5 and multiplied by the $[O_2]$ of air-equilibrated water obtains the concentration of oxygen dissolved in the sample at a given point in time. The first absorbance at 576 nm started at 0 seconds and repeated every 14.8 seconds over the course of 1600 seconds.

The Adair constants K_1-K_4 were determined using Gill's ingenious equations.[50] First, the absorbance changes at 576 nm in the ICAM+milk were used to determine the franctional saturation of hemoglobin within the erythrocyte using the earlier equation:

(13) $$\bar{Y} = [Abs_x - Abs_0]/[Abs_\infty - Abs_0]$$

where $\bar{Y}$ represents the fractional saturation of the hemoglobin within the erythrocyte, Abs_x represents the equivalent absorbance per centimeter of the hemoglobin within the erythrocyte at a given point in time, Abs_0 is the equivalent absorbance per centimeter of

fully deoxygenated hemoglobin within the erythrocyte, and Abs_{∞} is the equivalent absorbance per centimeter of fully oxygenated hemoglobin within the erythrocyte. The measured absorbance in the ICAM+milk follow a non-linear relationship with respect to concentration. Due to this, the measured absorbances at 576 nm in the ICAM+milk were transformed to equivalent absorbance per centimeter using the reversed transfer function (*eq. 8*):

(8)
$$x = -\frac{\ln(\frac{-y}{0.9375}+1)}{40.03}$$

where *y* is the measured absorbance in the ICAM, and *x* is the equivalent absorbance per centimeter. In this manner, the measured absorbances at 576 nm ranging from 0.453 to 0.329 were transformed to equivalent absorbance per centimeter ranging from 0.0165 to 0.0108. The equivalent absorbance at 576 nm for deoxygenated hemoglobin within the erythrocyte, or Abs_0, was determined experimentally with the addition of dithionite at very low concentrations of oxygen. The equivalent absorbance at 576 nm for fully oxygenated hemoglobin within the erythrocyte, or Abs_{∞}, was found by extrapolation. In order to determine Abs_{∞}, a double-reciprocal plot was used plotting the inverse of *F* (*eqs. 14-16*) against the inverse of oxygen concentration, *1/[x]*, using the data points for the top 10% of absorbances *(fig. 4.6*). When a linear fit of the double-reciprocal plot is compared to equation 16, the *y*-intercept is *A* from equation 15. When *A* is added to the known Abs_0, Abs_{∞} is obtained. When Abs_x, Abs_0, and Abs_{∞} are used with equation 2, the fractional saturation of hemoglobin with the erythrocyte can be determined. The slope of

the double-reciprocal plot can be used to determine S_2 of Gill, the upper limiting slope, which can be used in equation 17 to determine K_4.

(14) $$F = Abs_x - Abs_0$$

(15) $$A = Abs_\infty - Abs_0$$

(16) $$\frac{1}{F} = \frac{1}{A} + \frac{1}{AS_2} * \frac{1}{x}$$

(17) $$S_2 = 1/[4 * K_4]$$

With the fractional saturation obtained for any value of Abs_x, the plot of the fractional saturation versus oxygen concentration using data from the bottom 25% of the fractional saturation curvecan be used to determine the first two Adair constants, K_1 and K_2. The fractional saturation was plotted against oxygen concentration and fitted with a quadratic equation with the *y*-intercept at 0 (*fig. 4.7*). The fit can be used to determine the Gill parameters S_1 and C_1 from equation 18,

(18) $$\frac{[Abs_x - Abs_0]}{[Abs_\infty - Abs_0]} = S_1 x * C_1 x^2$$

where S_1 is a limiting slope and C_1 is the curvature at the bottom of the oxygen binding curve. The Adair constants K_1 and K_2 can be found directly from S_1 and C_1 using equations 19 and 20.

(19) $$S_1 = K_1/4$$

(20) $$C_1 = \left[2K_1K_2 - {K_1}^2\right]/4$$

The next two parameters, the Hill number, n_H and the concentration of oxygen at half-saturation, or $\bar{X}$, were determined using the Hill plot (*fig. 4.5*). The Adair constant K_3 was determined through a univariate fit of equation 1 using Graphpad (*fig. 4.8*). Figure 4.8 shows the Adair constant curve fit versus experimental data.

	Hemoglobin within Erythrocytes
Abs_0	0.0107
Abs_∞	0.0167 ± 0.00013
K_4	2.7306 ± 0.3684
K_1	0.0353 ± 0.00638
K_2	0.0878 ± 0.0144623
$\bar{X}$	23.28 ± 4.6μM
n_H	2.036 ± 0.1155
K_3	0.000448 ± 0.0000378

Table 3.1: Parameters for Oxygen Binding to Hemoglobin within the Erythrocyte Determined at 576 nm

Adair constants with the two parameters used for the oxygen binding curve fit are compared to literature values.

The preliminary data show weaker oxygen binding of oxygen-to-hemoglobin within the erythrocyte at lower oxygen concentrations when compared to hemoglobin in solution. This corresponds to more efficient delivery of oxygen to tissues under high oxygen demand. Our data also show the oxygen binding at higher oxygen concentration is tighter than hemoglobin in solution, for a more efficient uptake of oxygen for the erythrocytes in the lungs. During the spectrophotometry studies of hemoglobin, the heme concentration was kept above 150 μM to ensure the $\alpha_2\beta_2$ tetramer does not dissociate to αβ dimers.[45] The intracellular hemoglobin concentration inside human erythrocytes is 20 mM, and the concentration within the crystal is 40 mM. The R/T conformational change cannot be accommodated within the same crystal lattice. Inter-tetramer distances within the erythrocyte are only 25% longer than in the crystal, perhaps the minimum needed for the R/T conformational change. There are clear functional differences in the hemoglobin tetramer within the erythrocyte versus in solution that correlate with the difference in packing.

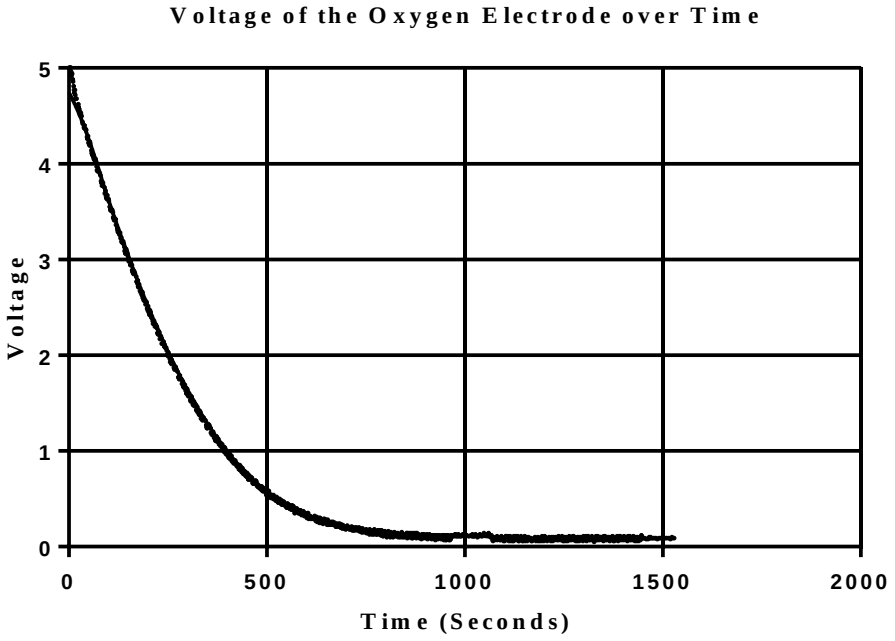

Figure 4.2: Oxygen Electrode Measurements

The function $\boldsymbol{f(x) = Ax^4 + Bx^3 + Cx^2 + Dx + E}$ was used to fit the 1529 data points of voltage over time during the deoxygenation of erythrocytes. The curve fit uses $A = 1.781 * 10^{-12}$; $B = -9.79 * 10^{-9}$; $C = 1.933 * 10^{-5}$; and $D = -0.01634$; and E equals 5.096, with $\sigma_{fit} = 0.0117$.

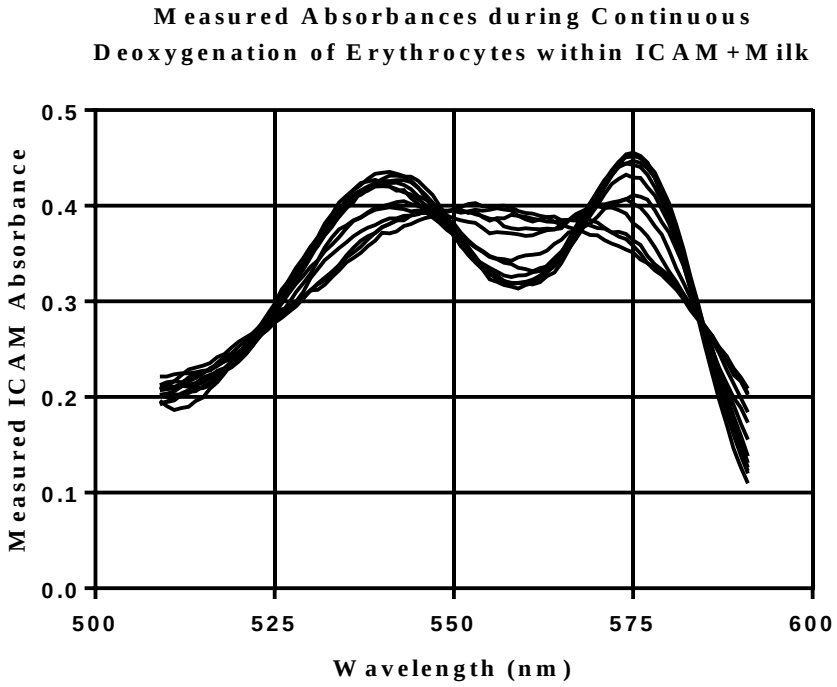

Figure 4.3: Measured ICAM Absorbances during Continuous Deoxygenation of Erythrocytes within ICAM+Milk

Every 5th scan for the ICAM is shown for clarity. The measured ICAM absorbances were transferred to equivalent absorbance cm^{-1} using the reversed transfer function (*eq. 8*) for ICAM+milk (*fig. 4.4*).

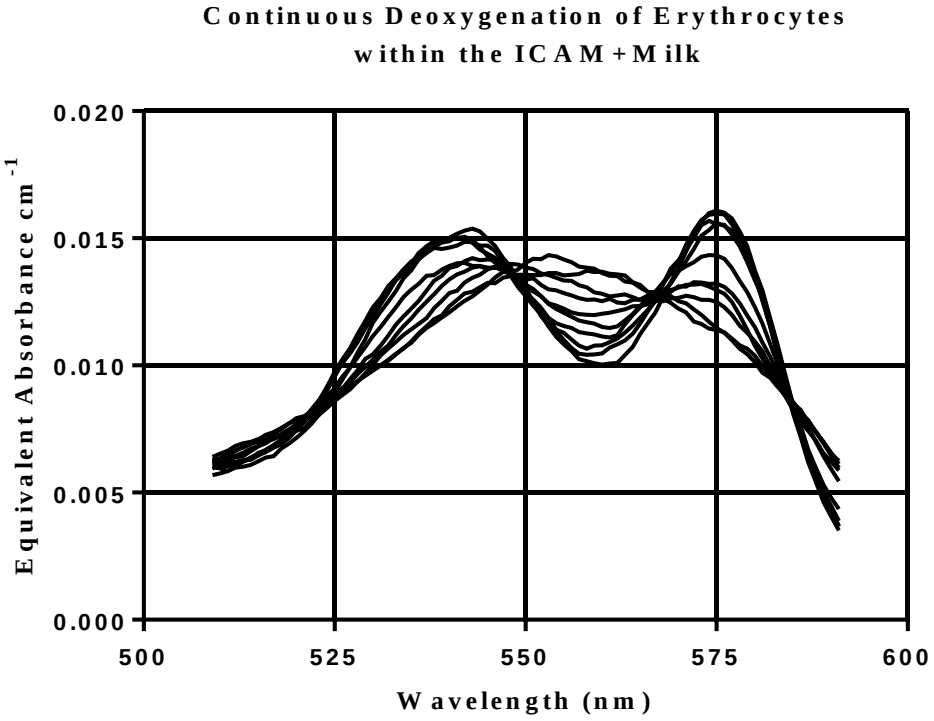

Figure 4.4: Equivalent Absorbances during Continuous Deoxygenation of Erythrocytes within the ICAM+Milk

Every 20th scan for the ICAM is shown for clarity. The measured absorbances (*fig. 4.3*) were transformed with equation 8 to calculate the equivalent absorbance cm^{-1} at 576 nm.

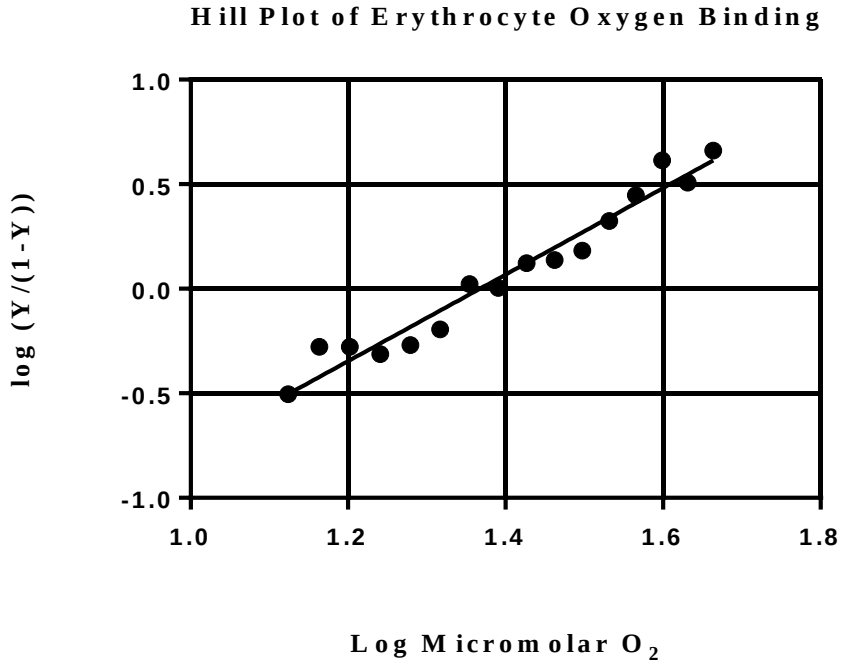

Figure 4.5: Hill Plot of Oxygen Binding to Hemoglobin within the Erthryocyte

The Hill equation was fitted to the data at half-saturation from $\bar{Y}$ at 0.821 to 0.218 with a linear fit $f(x) = mx + b$, where *x* is the log of oxygen concentration, *m* equals 2.071 ± 0.1155, and *b* equals -2.831 ± 0.1632. The Hill coefficient, n_H was 2.071 ± 0.1155 by least-square, and the half-saturation $\bar{X}$ was 23.2 ± 4.6 μM. $\sigma_{fit} = 0.0761$

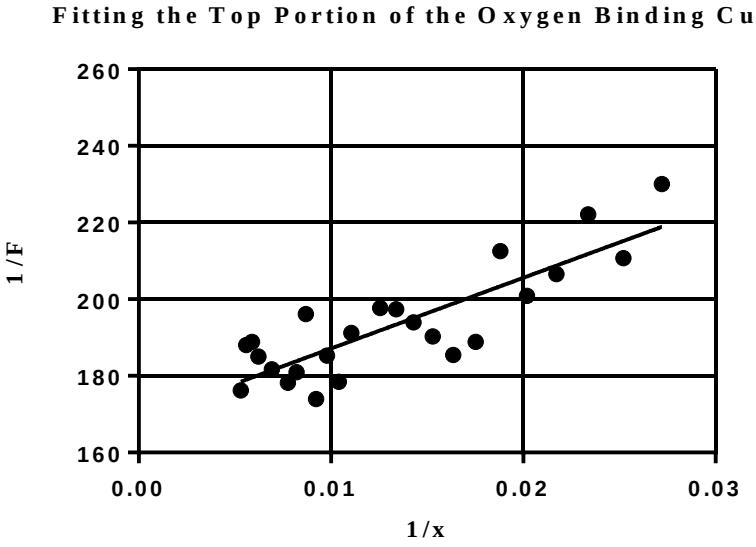

Figure 4.6: Fitting the Top 10% Portion of the Oxygen Binding Curve

The top 27 fractional saturation data points were used to find both Abs_∞ and S_2 by a double reciprocal plot of *1/F* vs. *1/x*, where $\boldsymbol{F = Abs_x - Abs_0}$ and *x* is the oxygen concentration in µM. A linear fit with $\frac{1}{F} = \frac{1}{A} + \frac{1}{AS_2} * \frac{1}{X}$ gives the values of Abs_∞ and S_2 using equations 13-15. The linear fit of $\boldsymbol{f(x) = mx + b}$ gave m = 1845 ± 249.2, and b = 168.7 ± 3.703. Calculations using equations 14-17 gave $Abs\infty$ = 0.0167 ± 0.00013. The Gill parameter S_2 could be determined using the linear fit, and equation 17 with S_2 determined K_4 = 2.7306 ± 0.3684. σ_{fit} = 7.909

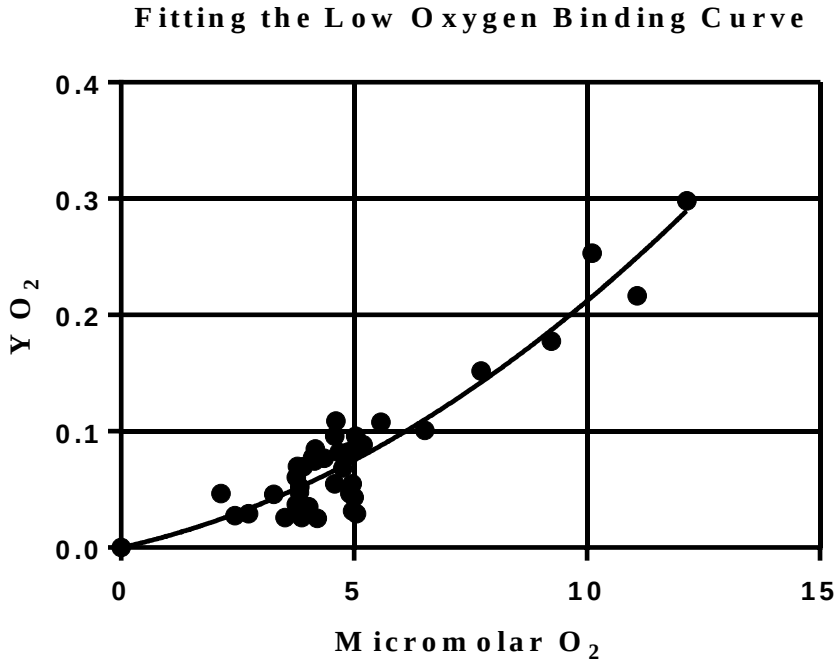

Figure 4.7: Fitting the Low Portion of the Oxygen Binding Curve

Determining S_1 and C_1 from the curve fit $\boldsymbol{f(x) = S_1 x + C_1 x^2}$. S_1 was equal to 0.008818 ± 0.01601, while C_1 was equal to 0.001238 ± 0.0002044. Using the Gill equations, these can be used to calculate K_1 and K_2. σ_{fit} = 0.02202

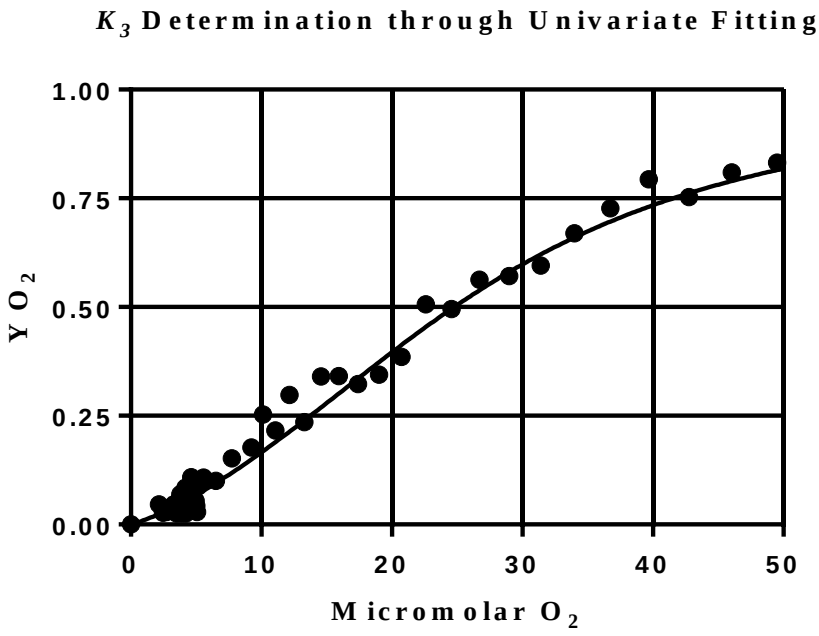

Figure 4.8: K_3 Determination through Univariate Fitting

This figure shows the calculated oxygen binding curve using the Adair constants with univariate fitting to determine $K_3 = 0.000448 \pm 0.0000378$, with $\sigma_{fit} = 0.04933$.

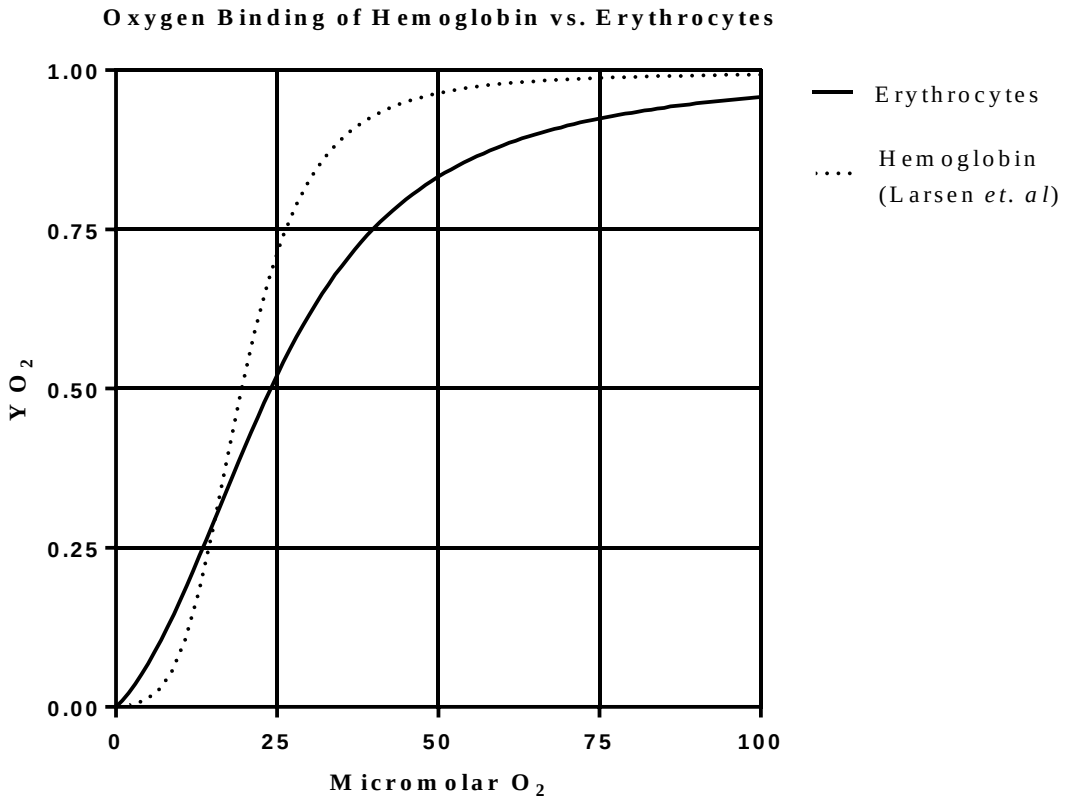

Figure 4.9: Oxygen Binding of Human Hemoglobin in Solution vs. within the Erythrocyte

The oxygen binding curve of human hemoglobin within the erythrocyte was determined at pH 6.8 and 22ºC, and compared to literature values.

Chapter 5 Future Directions and Conclusions

Marked functional differences between the hemoglobin in solution and the hemoglobin within the erythrocyte have been shown and quantified. It is now important to determine the binding free energies and enthalpies at the normal body temperature of 37ºC. Continued studies of adult human hemoglobin ranging over pH and temperature should also be done with Parkhurst's multiple wavelength global analysis. This will give the complete thermodynamic description of oxygen binding in normal human hemoglobin within the erythrocyte.

Thermodynamic studies of disease state erythrocytes, such as sickle-cell anemia (HbS), are expected to give new insight into the disease states of hemoglobin. HbS hemoglobin showed high cooperativity with unusually large concentration-dependent Hill coefficients.[51] However, this conclusion has been questioned.[52] The thermodynamics of oxygen binding with hemoglobin S are highly concentration dependent. The spectrophotometry of hemoglobin S required polymers and linkage theory to ensure the dimerization of hemoglobin does not occur in solution while the hemoglobin S is in close interaction with other tetramers. Studies of HbS within the erythrocyte would give clarity of the concentration-dependent thermodynamics of sickle-cell anemia.

Different iterations of the ICAM could also be explored. Parkhurst's derivations of the ICAM-milk showed the curve fit to be an exponential complement, which were shown in chapter 1. The derivations for a cube have also been deduced, and for a cuvette with reflective walls designed by 3D printing.

Appendix A Apparatus Holder Design

A.I Introduction

Early in the studies with the ICAM roundbottom flask, the ICAM was housed in a very simple apparatus in the sample chamber. That apparatus showed noticeable absorbance changes over time due to a shift of the ICAM during operation. Due to these flaws, a new apparatus was designed to eliminate absorbance drift.

A.II Materials and Methods

The initial design of the ICAM system utilized a 250 mL roundbottom flask coated on its outer surface with a flat white paint. A pneumatically driven magnetic stir plate was set into the instrument sample chamber with a cork roundbottom flask holder to hold the ICAM when in operation. The incident light traveled through the ICAM and was scattered, while the reference beam in the Cary 300 was kept in the same logarithmic range as the incidence beam by use of a neutral density filter.

To determine the instrument noise with this setup, the ICAM was zeroed and blanked with 270 mL 50 mM phosphate buffer, pH 6.8, with the baffle in place. Afterwards, 1000 μL of 1 mM hemoglobin solution was added to the ICAM, and 1000 scans were run over the course of 150 minutes. Figure A.1 shows 10 spectra, each representative of 100 scans smoothed by a 9 point quadratic Savitzky-Golay filter, and averaged together. Unfortunately, there was a loss of absorbance due to movement of the ICAM in the initial apparatus. It was decided a new ICAM apparatus holder needed to be

designed. The new apparatus holder was designed out of aluminum using kinematic design principles.[53] The new design was tested to determine if the absorbance reading at 576 nm was stable over the course of 1000 scans using 270 mL 50 mM phosphate buffer, pH 6.8 with 1000 µL 652 mM human hemoglobin, and the ICAM did not move during operation.

A.III Results and Discussion

The measured absorbances in the ICAM-milk before the new apparatus holder was built showed a steady decrease in absorbance over the course of the 150 minutes due to ICAM slippage (*fig. A.1*). The instrument was unstable, constantly shifting on top of the cork holder. When the new ICAM apparatus holder was introduced, there was no change in absorbance over the course of the 150 minutes (*fig. A.2*).

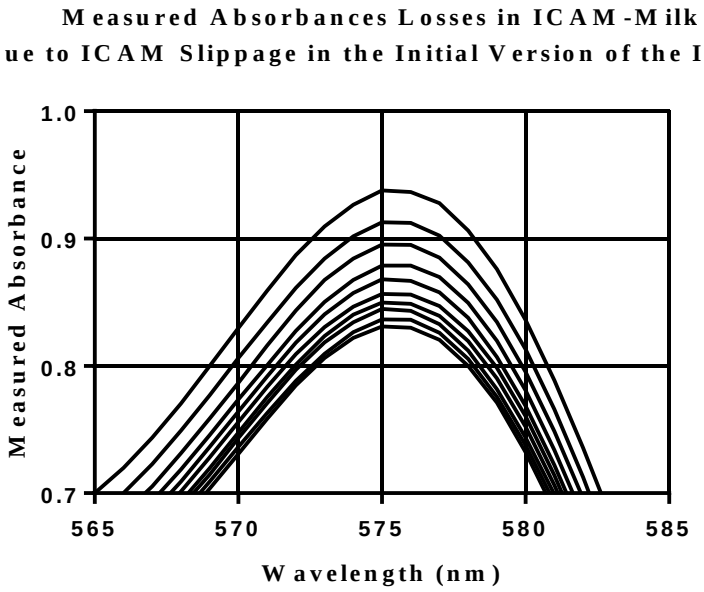

Figure A.1: Measured Absorbance in ICAM-Milk Due to ICAM Slippage in the Initial Version of the ICAM

A loss of absorbance at 576 nm was noticed when 1000 scans of hemoglobin were each 9 point quadratic Savitzky-Golay filtered, then averaged into groups of 100. This steady loss was due to the progressive movement of the ICAM.

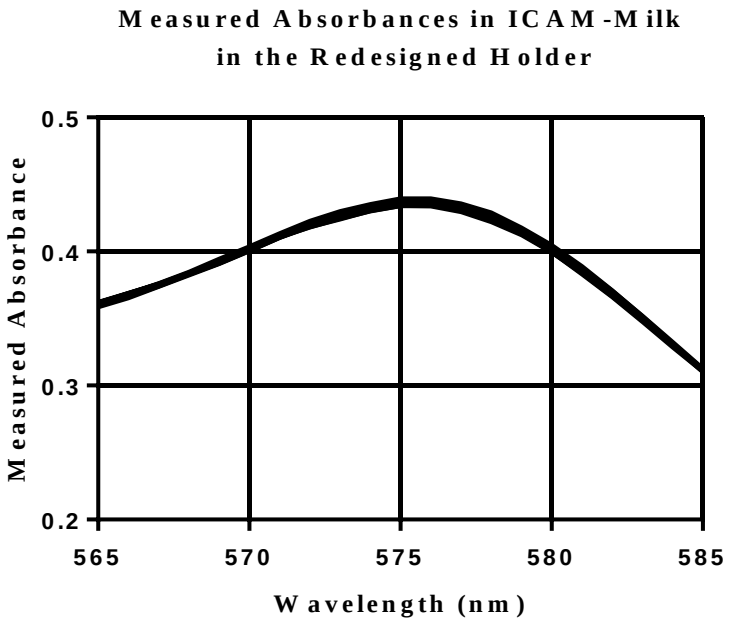

Figure A.2: Stability of the New ICAM Holder

The ICAM was placed in the new holder and its change of absorbance over time was test using 270 mL 50 mM phosphate buffer, pH 6.8 with 1 mL of 652 mM hemoglobin. This showed no change over time.

Appendix B Settings of the ICAM

During the final experiments, the standard procedure was to run the experiment from 600 nm to 500 nm unless otherwise stated. The stepper motor in the Cary 300 stepped every 1 nm (λ). The minimum time for an absorbance measurement was set by the speed of the double choppers. The time for an absorbance measurement at each wavelength was set to 66 milliseconds. The Cary 300 stepper motor would scan from 600 nm to 500 nm (unless otherwise stated) in the course of 12 seconds. The stepper motor would slew from 500 nm back to 600 nm with no absorbance measurements taken during this time. The slewing took 2.8 seconds. The timings of the stepper motor were determined through direct observation from numerous consecutive runs.

The stirring speed was controlled by the pressure of the air flowing through the pneumatically driven magnetic stir plate. The highest pressure allowed without any wobbling was 18 PSI. In order to ensure consistent stir speeds, the revolutions per second in the ICAM were determined by holding a stethoscope to the neck of the ICAM and attaching the earpiece to a microphone recording the sound. A freeware Winscope program developed by Andy Collinson sampled input waveforms from a computer's microphone measurements.[54] The sample was stirred by a Teflon coated magnet at a constant speed of 2.7 revolutions per second to ensure a homogenous solution within the ICAM during its operation (*fig. B.1*). The stirring dead time was determined by adding a sample of metmyoglobin into the ICAM+milk via a syringe. The metmyoglobin spectrum was constant within 1.1 seconds (*fig. B.2*). Due to the short dead time, no corrections for the stirring dead time were necessary.

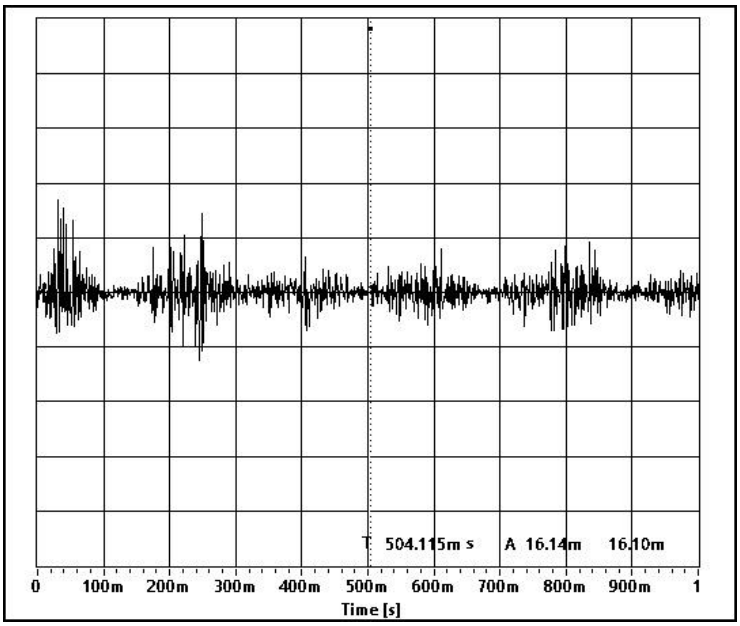

Figure B.1: Oscilloscope Microphone Measurements at 18 PSI

Each grouping represents a half-turn of the stir bar in the ICAM at 18 PSI. The distance between one set of peaks and the other was determined to be 0.185 seconds per half-turn, or 2.7 revolutions per second.

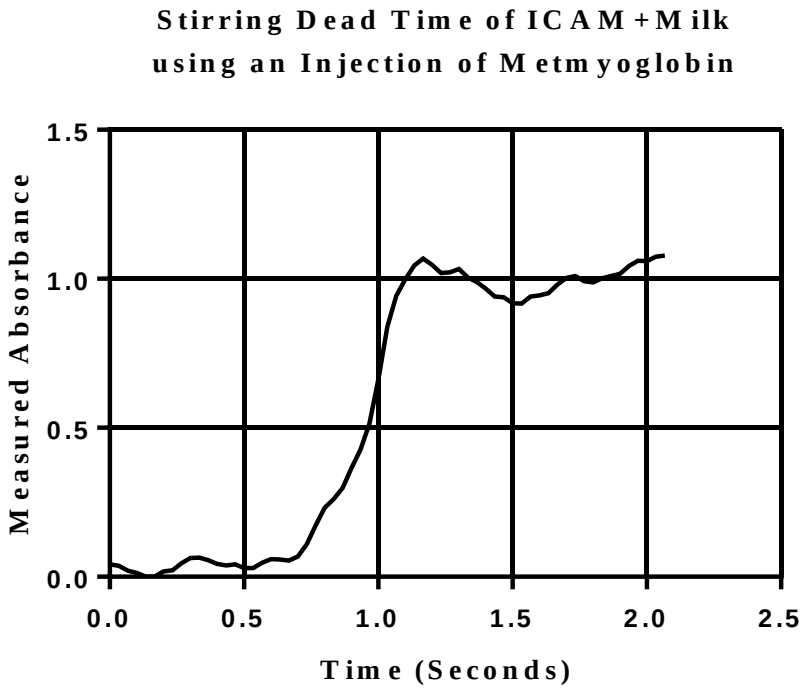

Figure B.2: Stirring Dead Time of ICAM+Milk

The stirring dead time was determined by using a solution of 462 µM metmyoglobin in 50 mM sodium phosphate, pH 8.0. The ICAM was blanked with 268.2 mL 50 mM sodium phosphate, pH 8.0 with 2.7 mL 1% milk. 1.7 mL of the metmyoglobin solution was injected into the ICAM+milk and the absorbance change at 500 nm recorded over time.

Appendix C Automated Oxygen Electrode

The oxygen concentration in the ICAM during the deoxygenation process was measured through a YSI 5300 oxygen electrode. The YSI oxygen electrode was a Clark electrode, which reduced oxygen and required stirring to maintain equilibrium with the electrode environment. The Clark oxygen electrode uses platinum-silver electrodes surrounded by potassium chloride and the electrode chamber separated from the reaction chamber by a Teflon membrane. The Teflon membrane was permeable to dissolved oxygen, and the electrodes generated a reaction with the oxygen being the limiting reagent. The reaction is $O_2 + 4\ e^- + H_2O \rightarrow 4\ OH^-$. The instrument was self-calibrating with analog measurements shown on the instrument's interface in terms of percentages. The instrument was set to 100% using air-equilibrated water. The calculation of the oxygen concentration for air-equilibrated water is in appendix V. The analog signal was converted to digital in order to ensure fast, precise oxygen concentration measurements. The conversion occurred using a Sparkfun Redboard microprocessor. A wire ran from the differential port on the YSI 5300 to the A_0 analog port on the Redboard, while another wire ran from the grounding port on the YSI 5300 to the grounding port on the Redboard. The Redboard was connected to a computer using a mini-USB port on the Redboard to a USB port on the computer. The Redboard was programmed using Arduino, a freeware program provided by Sparkfun (*see fig. C.1*).

```
/*
Analog-to-Digital
Reads an analog input on pin 0, converts it
to voltage, and prints the result to the serial
monitor.
*/

// the setup routine runs once when you
press reset:
void setup() {
// initialize serial communication at 9600
bits per second:
Serial.begin(9600);
}

// the loop routine runs over and over
void loop() {
// read input on analog pin 0:
int sensorValue = analogRead(A0);
// Convert the analog reading (which goes
from 0 - 1023) to a voltage (0 - 5V):
float voltage = sensorValue * (5.0 / 1023.0);
// print out:
Serial.println(voltage);
delay(1000);
}
```

Figure C.1: Arduino Program for the Oxygen Electrode

This program was programmed into the Redboard microprocessor. The microprocessor took the analog signal as a scale from 0-1023 bits, and converted it to digital signal as voltage (0-5V). The voltage could be transformed into percent relative oxygen by dividing by 5.

Appendix D Erythrocyte Storage, Retrieval, and Survival

D.I Introduction

Blood transfusion was the most important medical advance of World War I with the development of a citrate-glucose solution used to store blood.[55] At the time, however, it was not clear how to store frozen blood and later recover it. In the 1950s, Lovelock stated that the damage to red blood cells during the freezing and thawing process was due to the osmotic stress.[56] Shortly after, Smith, working with Polge, discovered glycerol as the first practical cryoprotectant molecule, and used it to cryopreserve, thaw, and subsequently wash the red blood cells free of cryoprotectants.[57,58] It was thought that the storage of red blood cells would eliminate the problems associated with erythrocyte suspensions in transfusion: seasonal shortages, rare blood types, and natural disasters. Two main groups of cryoprotectants have been developed, classified as "penetrating" and "non-penetrating."[59,60] The former, such as glycerol, invade the cell and change the osmotic equilibrium during freezing. In this way, the volume reduction due to intracellular ice formation is reduced. The second group of cryoprotectants form a shell around the erythrocyte in a process called vitrification, and in this way, protect the red blood cells from osmotic damage. During the freeze-thaw-wash (FTW) processing of red blood cells, there are two main problems. One of them is the initial lysis of red blood cells, and the second is the post-thawing survivability of the red blood cells. If enough osmotic damage occurs, or if the cell function is limited after post-FTW, or if the cell cannot maintain integrity in the thawing solution, then hemolysis will happen rapidly over the course of a few days. Our goal post-FTW is focused on the latter. We make the

assumption that post-FTW survivability indicates the RBC are more physiologically relevant.

The goal of post-FTW survivability is based upon post 24-hour transfusion survival rates. National Academy of Science NRC has arbitrarily established a survival of 70% in 24 hours post-transfusion as the acceptable level for the viability of preserved erythrocytes. For our work, we arbitrarily set our goal as less than 1% per day. This would ensure a sample that would remain relatively stable over the course of 2-3 weeks. We found that using 40% (v/v) glycerol as a cryoprotectant and using AS-3 storage buffer (100 mL H_2O, 1.10g of dextrose monohydrate, 0.558g of sodium citrate dihydrate, 0.276 g of monobasic sodium phosphate monohydrate, 0.42 g of citric acid monohydrate, and 0.030 g of adenine) offered our samples three-weeks of adequate post freeze-thaw-wash survival at 4ºC.[61,62]

D.II Materials and Methods

Initially, our work began with Flegel's work at the NIH, who focused on using polyvinyl pyrrolidone (PVP) as a non-invasive cryoprotectant (16). Human blood from KH or LJP was collected into concentrated ethylenediaminetetraacetic acid, and stored at 4ºC. The samples were centrifuged at 1000xg for 5 minutes to isolate the red blood cells. The packed RBC samples had the supernatant removed, and the lost volume replaced with 1% w/v NaCl, 50 mM sodium phosphate buffer pH 6.8 (PBS buffer). This process was repeated until the supernatant was clear. The packed red blood cells were cryoprotected in one of two ways: fast-freezing through non-invasive cryoprotectants, and slow-freezing through invasive cryoprotectants.

With the non-invasive cryoprotectants, one volume of packed erythrocytes was introduced into one volume of PVP freezing solution (27mL of 30% w/v bovine serum albumin with 23% (v/v PVP in deionized H_2O). The mixture was allowed to equilibrate for 1 hour. Afterwards, the mixture was pipetted dropwise into a liquid nitrogen-filled Dewar flask. These droplets were collected with a metal spatula, and placed into a cryovial tube with the top punctured several times. Both the cryovial tubes and the metal spatula were chilled with liquid nitrogen beforehand to ensure the droplets didn't thaw and stick on contact. Afterwards, the cryovial tubes were placed into the -80ºC freezer until thawed.

During the thawing process, the desired amounts of droplets (around 80-160 µL each) were placed into 1.5 mL of PBS buffer at 37ºC with gentle shaking. After complete suspension, the sample was washed with storage buffer at 3 fold-excess until no hemolysis occurred (around 2-3 washes). This lowered the PVP left in solution to approximately 0.0001 M. Afterwards, the red blood cells were resuspended, aliquoted into individual-use Eppendorf tubes and placed into 4ºC storage until use. The two storage buffers used were 1% PBS buffer and AS-3 solution.

Valeri's work with the Naval Blood Research Laboratory focused on invasive cryoprotectants.[61,62] Two volumes of a glycerol freezing solution (50% w/v glycerol, 1% w/v 2-hydroxy-propanoic acid, 1% w/v KCl, 50 mM sodium phosphate buffer, pH 6.8) were added for every volume of packed red blood cells. The mixture was allowed to equilibrate for 1 hour. Afterwards, the mixture was aliquoted into cryovials, and the temperature was lowered at 1ºC/min by insulating the test tubes in a room-temperature

Styrofoam box, which was placed into the freezer and the temperature checked every hour until -80ºC was reached.

Two different thawing procedures were used to remove the intracellular glycerol. The frozen glycerolized samples were warmed to 37ºC. Afterwards, the samples were centrifuged at 1000xg and the supernatant removed. 1 volume of 12% PBS buffer was added dropwise to 3 volumes of the thawed RBC sample with gentle mixing, and equilibrated at room temperature for 3 minutes. Afterwards, 3 volumes of 0.2% dextrose (w/v), 0.9% saline (w/v) was added dropwise with gentle shaking, then left to equilibrate for 3 minutes, and this process was repeated 4 times. At this point, the sample was centrifuged for 3 minutes at 1000xg, and then an eighth of the total volume was aspirated, replaced with storage buffer, then the packed RBC were resuspended. This process was repeated 8 times, with the following volumes aspirated and replaced: $1/8^{th}$, $1/4^{th}$, $3/8^{th}$, ½, and finally $4/5^{th}$. Afterwards, the RBC samples were aliquoted into one-use Eppendorf tubes and placed into the 4ºC refrigerator. The two storage buffers used were 1% PBS buffer and AS-3 solution.

D.III Results and Discussion

Hemolysis rates were measured by removing the sample from the 4ºC refridgerator and centrifuging the sample for 3 minutes at 1000xg. The supernatant was removed and placed in a pre-tared Eppendorf tube. The packed erythrocytes were resuspended using storage buffer. Both samples were massed, and the density assumed to be 1g/mL. Both of these solutions had 10-100 µL removed and placed into 2 mL deionized H_2O. The absorbances at 578 nm for both of these diluted solutions were

measured and their final concentrations measured. The total heme lysed versus the total heme in cells give us the total hemolysis and total survival.

We assume that higher post-FTW survival indicates the RBC are more likely to be physiologically relevant. Based on our results, we decided that using Valeri's methods with glycerol and AS-3 solutions would be most effective as compared to Flegel's method with polyvinylpyrrolidone. Personal contact with Flegel and Valeri, revealed that their aims were different. Valeri was focused on survival rates post FTW at 4ºC due to his career's work with the US naval research laboratories. He was focused on keeping rare blood types viable on warships for long periods of time. Flegel, on the other hand, focused his work on laboratories using the thawed red blood cells on that given day, and focused on quick and efficient methods to thaw erythrocytes for a single day's use.

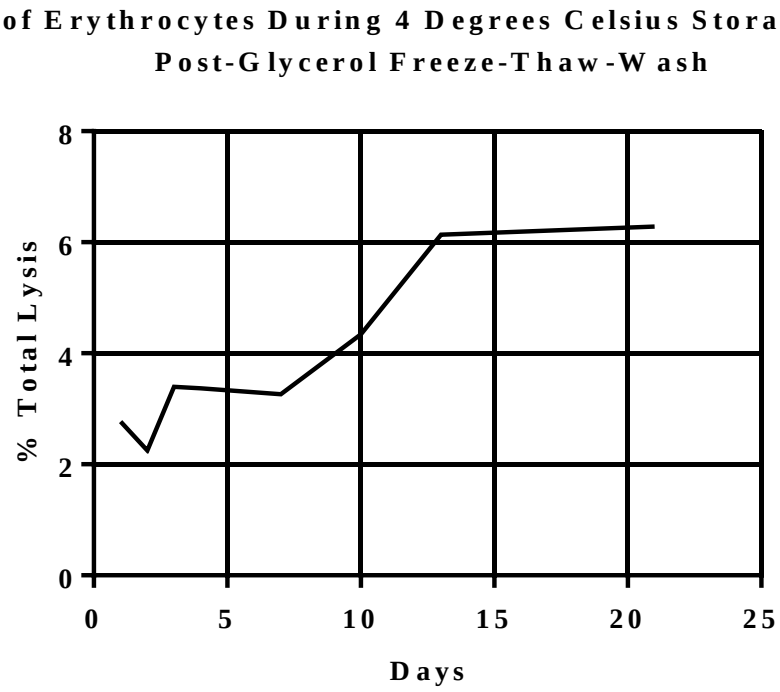

Figure D.1: Lysis of Erythrocytes During 4 Degrees Celsius Storage in AS-3 Post-Glycerol Freeze-Thaw-Wash

Valeri's methods of erythrocyte storage and retrieval using glycerol as a cryoprotectant for the erythrocytes at -80ºC followed by AS-3 solution in the erythrocyte suspension at 4ºC proved adequate for three weeks.

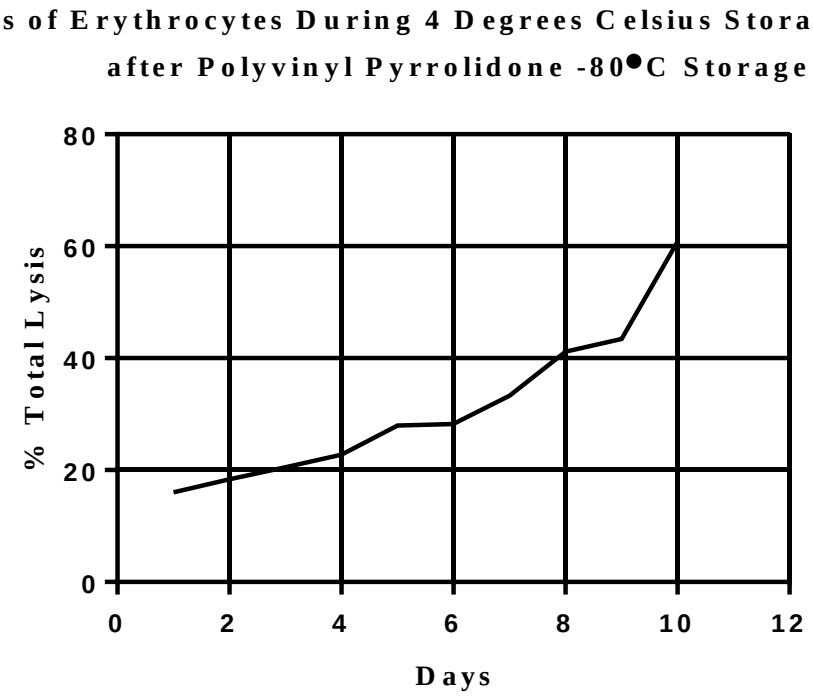

Figure D.2: Lysis of Erythrocytes During 4 Degrees Celsius Storage in PBS after Post-Polyvinyl Pyrrolidone -80ºC Storage

Ten days after retrieval from -80ºC storage, 60% of the erythrocytes had lysed in 4ºC PBS buffer.

Appendix E Dissolved Oxygen Calculations

In order to determine the concentration of air-equilibrated water, the true air pressure and temperature were recorded. The temperature of the lab was recorded with a thermometer. The air pressure and humidity were given by KLNK airport. The lab was determined to be 75 feet above KLNK airport. The true air pressure was given determined by:

(21) $$Lab\ Air\ Pressure = \left[KLNK + \left(75\ feet * \frac{26\ mmHg}{1000\ feet\ above\ sea\ level}\right)\right]$$

The oxygen activity can be determined using the gas solubility tables.

(22) $$X_A = \frac{\alpha^T(0.20946)}{R(273.18)} * \frac{P^b - P^T H}{760\ mmHg/Atm}$$

Where: α^T = the volume of oxygen in liters absorbed by one volume of water when the pressure of the gas itself amounts to 760 mm.[63]

R = 0.082054 liter atm. deg.$^{-1}$ mol^{-1}

P^b = ambient lab air pressure in mmHg

P^T = ambient pressure of water at a temperature read from the table

H = ambient %relative humidity divided by 100.

References

(1) Perutz, M.; Steinrauf, L.; Stockell, A.; Bangham, A. *Journal of Molecular Biology* **1959**, *1*, 402.

(2) Muirhead, H.; Perutz, M. *Nature* **1963**, *199*.

(3) Perutz, M. *Unravelling the Atomic Mechanism of Haemoglobin*; World Scientific, 1997.

(4) Perutz, M. F.; Wilkinson, A.; Paoli, M.; Dodson, G. *Annual Review of Biophysics and Biomolecular Structure* **1998**, *27*, 1.

(5) Bellelli, A.; Brunori, M. *Biochimica et Biophysica Acta (BBA)-Bioenergetics* **2011**, *1807*, 1262.

(6) Engelhart, J. F. *Commentatio de Vera Materiae Sanguini Purpureum Colorem Impertientis Natura*; Typis Dieterichianis, 1825.

(7) Bert, P. *La Pression Barométrique*; G. Masson, 1878.

(8) Haldane, J. S.; Priestly, J. G. *Press, New Haven Conn* **1922**.

(9) Barcroft, J.; King, W. O. R. *The Journal of Physiology* **1909**, *39*, 374.

(10) Adair, G. *Biological Reviews* **1924**, *1*, 75.

(11) Adair, G. S. *Journal of Biological Chemistry* **1925**, *63*, 529.

(12) Roughton, F. J. W. i.; Scholander, P. F. *Journal of Biological Chemistry* **1943**, *148*, 541.

(13) Van Slyke, D. D.; Neill, J. M. *Journal of Biological Chemistry* **1924**, *61*, 523.

(14) Roughton, F. J. W.; Otis, A. B.; Lyster, R. L. J. *Proceedings of the Royal Society of London B: Biological Sciences* **1955**, *144*, 29.

(15) Knowles, F. C.; Gibson, Q. H. *Analytical Biochemistry* **1976**, *76*, 458.

(16) Sick, H.; Gersonde, K. *Analytical Biochemistry* **1972**, *47*, 46.

(17) Imai, K.; Morimoto, H.; Kotani, M.; Watari, H.; Hirata, W.; Kuroda, M. *Biochimica et Biophysica Acta (BBA)-Protein Structure* **1970**, *200*, 189.

(18) Imai, K. *Allosteric Effects in Haemoglobin*; Cambridge University Press, 1982.

(19) Larsen, T. M.; Mueser, T. C.; Parkhurst, L. J. *Analytical Biochemistry* **1991**, *197*, 231.

(20) Fujisawa, H.; Hiromi, K.; Uyeda, M.; Okuno, S.; Nozaki, M.; Hayaishi, O. *Journal of Biological Chemistry* **1972**, *247*, 4422.

(21) Ohlendorf, D. H.; Lipscomb, J. D.; Weber, P. C. *Nature* **1988**, *336*, 403.

(22) Rifkind, J.; Lumry, R.; 2 ed.; Federation Amer Soc Exp Biol; Vol. 26, p 673.

(23) Nasuda-Kouyama, A.; Tachibana, H.; Wada, A. *Journal of Molecular Biology* **1983**, *164*, 451.

(24) Anderson, N. M.; Sekelj, P. *Physics in Medicine and Biology* **1967**, *12*, 173.

(25) Stover, J. C. *Optical Scattering: Measurement and Analysis*; Optical Engineering Press, 1995; Vol. 2.

(26) Clarke, A. D. *Applied Optics* **1982**, *21*, 3011.

(27) Lambert, J. H. *Acta Helvetica* **1758**, *3*, 128.

(28) Röttgers, R.; Häse, C.; Doerffer, R. *Limnol. Oceanogr. Methods* **2007**, *5*, 1.

(29) Khalizov, A. F.; Xue, H.; Wang, L.; Zheng, J.; Zhang, R. *The Journal of Physical Chemistry A* **2009**, *113*, 1066.

(30) Walsh, J. W. T. *Photometry*; Constable, 1953.

(31) Elterman, P. *Applied Optics* **1970**, *9*, 2140.

(32) Jávorfi, T.; Erostyák, J.; Gál, J.; Buzády, A.; Menczel, L.; Garab, G.; Naqvi, K. R. *Journal of Photochemistry and Photobiology B: Biology* **2006**, *82*, 127.

(33) Fry, E. S.; Kattawar, G. W.; Pope, R. M. *Applied Optics* **1992**, *31*, 2055.

(34) Mie, G. *Ann. Phys* **1908**, *25*, 337.

(35) Schenkman, K. A.; Marble, D. R.; Burns, D. H.; Feigl, E. O. *Journal of Applied Physiology* **1997**, *82*, 86.

(36) Clark, L. C.; Wolf, R.; Granger, D.; Taylor, Z. *Journal of Applied Physiology* **1953**, *6*, 189.

(37) Furse, J. *Journal of Physics E: Scientific Instruments* **1981**, *14*, 264.

(38) Dewan, R.; Chudgar, A.; Mead, R.; Bloomfield, V.; Morr, C. *Biochimica et Biophysica Acta (BBA)-Protein Structure* **1974**, *342*, 313.

(39) Wiking, L.; Stagsted, J.; Björck, L.; Nielsen, J. H. *International Dairy Journal* **2004**, *14*, 909.

(40) Glantz, M.; Håkansson, A.; Lindmark Månsson, H.; Paulsson, M.; Nilsson, L. *Langmuir* **2010**, *26*, 12585.

(41) Bowen, W. J. *Journal of Biological Chemistry* **1949**, *179*, 235.

(42) Motulsky, H. *Analyzing Data with GraphPad Prism*; GraphPad Software Incorporated, 1999.

(43) Parkhurst, L. J.; Gibson, Q. H. *Journal of Biological Chemistry* **1967**, *242*, 5762.

(44) Gray, R. D. *Journal of Biological Chemistry* **1974**, *249*, 2879.

(45) Guidotti, G.; Konigsberg, W.; Craig, L. C. *Proceedings of the National Academy of Sciences* **1963**, *50*, 774.

(46) Zijlstra, W.; Buursma, A. *Comparative Biochemistry and Physiology Part B: Biochemistry and Molecular Biology* **1997**, *118*, 743.

(47) Hill, A. V. *J Physiol (Lond)* **1910**, *40*, 4.

(48) Messerschmidt, A.; Ladenstein, R.; Huber, R.; Bolognesi, M.; Avigliano, L.; Petruzzelli, R.; Rossi, A.; Finazzi-Agró, A. *Journal of Molecular Biology* **1992**, *224*, 179.

(49) Kroneck, P. M.; Armstrong, F. A.; Merkle, H.; Marchesini, A. *Advances in Chemistry Series* **1982**.

(50) Gill, S. J.; Gaud, H. T.; Wyman, J.; Barisas, B. G. *Biophysical Chemistry* **1978**, *8*, 53.

(51) Gill, S. J.; Benedict, R. C.; Fall, L.; Spokane, R.; Wyman, J. *Journal of Molecular Biology* **1979**, *130*, 175.

(52) Eaton, W. A.; Henry, E. R.; Hofrichter, J.; Mozzarelli, A. *Nature Structural & Molecular Biology* **1999**, *6*, 351.

(53) Lee, T. W.; Freudenstein, F. *Journal of Engineering for Industry* **1976**, *98*, 1277.

(54) Cogswell, J. *Windows/DOS Developer's Journal* **1994**, *5*, 39.

(55) Chaplin, H., Jr. *Blood* **1982**, *59*, 1118.

(56) Lovelock, J. E. *Biochimica et Biophysica Acta* **1953**, *10*, 414.

(57) Smith, A. U. *The Lancet* **1950**, *256*, 910.

(58) Polge, C.; Smith, A. U.; Parkes, A. S. *Nature* **1949**, *164*, 666.

(59) Kim, H.; Tanaka, S.; Une, S.; Nakaichi, M.; Sumida, S.; Taura, Y. *Journal of Veterinary Medical Science* **2004**, *66*, 1543.

(60) Meryman, H. T. In *Transfusion Medicine: Quo Vadis? What Has Been Achieved, What Is to Be Expected*; Springer: 2001, p 69.

(61) Valeri, C. R.; Pivacek, L. E.; Cassidy, G. P.; Ragno, G. *Transfusion* **2000**, *40*, 1341.

(62) Valeri, C. R.; Ragno, G.; Pivacek, L.; O'Neill, E. M. *Transfusion* **2001**, *41*, 928.

(63) Haynes, W. M. *CRC handbook of chemistry and physics*; CRC press, 2014.